Pierre-Elouan RÉTHORÉ
s041541

Thrust and wake of a wind turbine: Relationship and measurements

M.Sc. thesis, September 2006

Preface

This thesis is submitted in partial fulfilment of the requirements for obtaining the M.Sc. degree in Wind Energy from the Technical University of Denmark (DTU). The project was carried on during the period between January and September 2006 at Risø National Laboratory, Roskilde, Denmark. The supervisors of the thesis were Martin O.L. Hansen at DTU and Sten T. Frandsen at Risø.

Acknowledgements

Many people contributed to this master thesis through knowledge, advises, data, literature, proof reading, and moral support.

At Risø: My supervisor, Sten T. Frandsen, as well as Rebecca Barthelmie, Uwe S. Paulsen, Kirsten H. Westermann, and Christian Jensen.

At DTU: My supervisor, Martin O.L. Hansen, as well as Kurt S. Hansen, and Jens N. Sørensen.

At Elsam: Leo E. Jensen and Martin Méchali.

At Siemens: Rune Rubak and Claus Balling.

Finally, my friends: Tim Fischer, Baptiste Berges, Imad Abdallah, Mark Capellaro, Ari Bronstein, David VanLuvanee, Guillaume Poirier, Hervé Utard, and Karen Marie Rasmussen.

Many thanks to all of you.

Pierre-Elouan Réthoré

Roskilde, September 2006

Nota Bene

▪ Data confidentiality

The measurements data used to validate the models were gathered from different sources (DTU, Risø, Siemens, Elsam, Energi E2) and are all only available under a confidentiality agreement with the specific owner of the data. Unfortunately, these data, and the resulting plots cannot be presented publicly. In order to make the general results of this report public, it was decided to presents the different results obtained with each data sets in separated confidential appendices, which are only meant for the specific owner of the data and for the examination of this master thesis by the supervisors of DTU and Risø. The global results presented in the public part of the report will therefore frequently reference for plots available in confidential appendices, which might not be necessarily available for the reader.

▪ Novelties of the report

The first two chapters contain a significant amount of theory gathered from various sources in the literature. While the sources are all referred properly, it can be sometimes difficult for the reader to identify the novelties presented in the report. Therefore, as a layout convention, only the new significant results will be presented in framed equations.

Abstract

The first part of the thesis stresses the importance of having an accurate knowledge of the thrust curve of wind turbines, in the context of estimating the production and lifetime of large wind turbine clusters. The second part of the thesis presents three methods to estimate the thrust curve of a wind turbine and apply them to real wind turbine data.

The first method uses wind speed measurements upstream and downstream a wind turbine to estimate the loss of momentum and to derive the thrust coefficient. The novelty of this method compared with the previous works found in the literature is to use a section of a cylinder control volume that takes into account the presence of the ground. The application of the method on real wind turbine measurement gives results in accordance with the thrust coefficient obtained from the wind turbine manufacturer. The accuracy of the result is not determined rigorously, but the relatively high variations between one wind speed bin to another indicates a large sensitivity of the result accuracy to the quality of wind speed measurement.

The second method uses bending moments measured by strain gauges located on the bottom part of a wind turbine's tower. The method also describe the estimation of the combined uncertainty of the thrust curve. Different scenarios of input uncertainties are analyzed. The results agree with the manufacturer thrust curves in term of magnitude and shape. The combined uncertainty of the thrust curve is found to be very dependent of the strain gauge standard uncertainty as well as the wind speed standard uncertainty.

Finally, the third method uses the Blade Element Method to derive the thrust curve. The novelty of the approach is, instead of using a model for the pitch and rotation speed control, the method uses real measurements inputs. The method is applied on an instrumented wind turbine using its airfoil data and sensors. The result, in comparison with the strain gauges measurement, gives a similar shape and much less scatter. The uncertainty with this method is found to be of a significantly smaller order of magnitude than the method using the strain gauges. Nonetheless, the uncertainty of the Blade Element Method is not considered, and is expected to increase significantly the combined uncertainty of the thrust curve.

Table of Contents

Introduction

The thrust is the axial force applied by the wind on the rotor of a wind turbine. Because all action yields an opposite reaction, the thrust is therefore also the axial force applied by the wind turbine on the wind. While the power output of a wind turbine describes only the amount of power transferred into the electrical system, the thrust is related to all the losses of kinetic energy of the flow, including the energy transformed into turbulent kinetic energy. For this reason, the thrust is used in most of the engineering models describing the flow in a wake of a wind turbine. Therefore, on a larger scale, the thrust is used to describe the production and the fatigue of wind turbines in clusters.

The wind energy industry is growing exponentially at all levels, in particular with respect to the size of the turbines, as well as the size of the wind parks. As the scale of the wind energy projects increase, the investments increase as well as the economical risks involved. Consequently, there is a growing demand, in the wind energy industry, for accurate means to estimate the production and the lifetime of large wind parks. As the existing models rely essentially on the power curve and the thrust coefficient curve of the turbines as inputs, their respective accuracies are critical to obtain realistic results. While the power curve accuracy has so far received a widespread interest, considerably less effort was put to analyze the thrust curve. For example, the IEC standards describe with precision how to measure the power curve and how to estimate its combined uncertainty. However, no such information is available concerning the thrust curve.

There is no direct way to measure the thrust of a turbine. The easiest way to estimate the thrust from measurements is to measure the bending moments on the tower and to estimate the thrust from them. However, calibrating strain gages on the tower with precision is relatively difficult, and the measurements are largely influenced by the vibrations of the tower. Therefore, the most common way to estimate it, in the wind industry, is to use a blade element code, relying on empirical airfoil data. This method, widely used to estimate the power curve, has been extensively compared with the real power output of turbines, as well as the forces applied on the blades. However, there was not any significant work found on a comparison between the estimated thrust, using this method, and the real thrust of a wind turbine. Therefore, the uncertainty of the thrust remains unknown with this method.

In this context, the aim of this thesis is to propose different methods to estimate the thrust force and its combined uncertainty from measurements. The first chapter is focused on setting up the fluid mechanics relationship between the thrust and the wind speed distribution in the wake of the turbine using different sets of assumptions. This relationship is used in chapter two to present a simple example on how the uncertainty of the thrust force can be propagated on the uncertainty of the wake wind speed. This chapter will also presents a link between the thrust of the turbine and the amount of turbulent kinetic power generated in its wake. Finally, the last chapter proposes three fundamentally different methods to estimate the thrust of a turbine from measurements. These methods are applied on different real wind turbines measurements and compared with the thrust curve given by the manufacturer, when available.

Chapter I
Equations of conservation in a wind turbine system

In this chapter, after the presentation of the different assumptions considered, the basic equations of momentum and energy conservation for a wind turbine system are derived, using both a rectangular and an axis-symmetric wake profile. The novelties of the approach, in comparison with what can be found in the literature, is mainly the usage of a section of a cylinder control volume in combination with the assumption of a self-similar axis-symmetric wake profile.

These results are used to give an expression relating the thrust coefficient and the power coefficient with the inflow and outflow characteristics. These relations are then used in Chapter II to present the importance of the accurate knowledge of the thrust and in Chapter III to develop a method estimating the thrust from wake measurements.

The theory developed here is slightly different from the actuator disc theory that is recalled in Appendix A. The main difference comes from the control volume which allow the momentum to go through its side face.

1 Assumptions

In order to be able to derive analytically the expression of momentum and energy conservation, some basic assumptions have to be made. These assumptions are a compromise between the realism of the system and the simplicity of the equations.

In this study, the assumptions taken will not differ considerably from the assumptions found in the literature, which have been used and discussed extensively. The only assumption taken that is not be found to be documented in the literature [Vermeer et al., 2003] is concerning the usage of a control volume defined as a section of a cylinder instead of the regular cylinder. While a more serious approach of the analysis of these assumptions can be found in the literature, a quick introduction of the assumptions and their limitations is presented to underline the degree of realism the models can reach.

1.1 Literature review

There has been extensive analysis of the wake profile behind a turbine. Most of the previous work done on the subject has recently been reviewed by Vermeer et al. [2003]. As it is pointed out, there has been an evolution of the approach regarding the wake analysis. The first approach was to

create semi empirical rules from observations (the so-called engineering rules). Their aim was to create basic security rules for the design of wind turbine, and wind farms. As the knowledge about wind energy has increased, and the design of the turbine changed (for example from Stall regulated turbine to Pitch regulated turbine), the research is now more and more directed toward a full scale study and trying to reduce the number of assumptions, and empirical values as much as possible.

For a wind turbine system, the assumptions taken in the literature are generally quite drastic: the influence of the ground is neglected, and the inflow and outflow are assumed to have a rectangular profile. These assumptions may be acceptable for a control volume relatively close to the wind turbine, as the one used in the actuator disc theory. However, they become more and more inaccurate with a larger control volume. In order to carry on the measurement validations of the models, the control volume becomes too big to neglect the presence of the ground in the equations; this results in the use of a different control volume than the usual cylindrical control volume taken in the literature.

1.2 Steady flow

A steady flow is a flow that is independent of the time. This assumption is generally used in order to drop the terms relative to the time derivative of wind speed. In reality, the wind is far from being steady. However, it can be argued that if it is taken on 10-minute average, with a low standard deviation, the assumption is acceptable. The idea behind this assumption is that there is not any change of the flow property going on, e.g. no gust, no wind direction change, and no temperature change.

The degree of validity of this assumption in measurements can be statistically controlled by excluding the time series where the standard deviations of the flow properties are relatively too large.

1.3 Section of a cylindrical control volume

Because of the disc shape of the rotor, the system has an axis symmetry, which can be used to simplify the equations. As it was briefly introduced, taking a cylindrical control volume is acceptable for a control volume very close to the rotor. However, if the wake behaviours have to be taken into account at a far distance downstream the turbine (>4 rotor diameters), the control volume becomes so big that it will eventually reach the ground level. In that case, parts of the inflow and outflow faces are underground, and should not be taken into account. For this reason, the control volume chosen is a section of a cylindrical control volume (Figure 1).

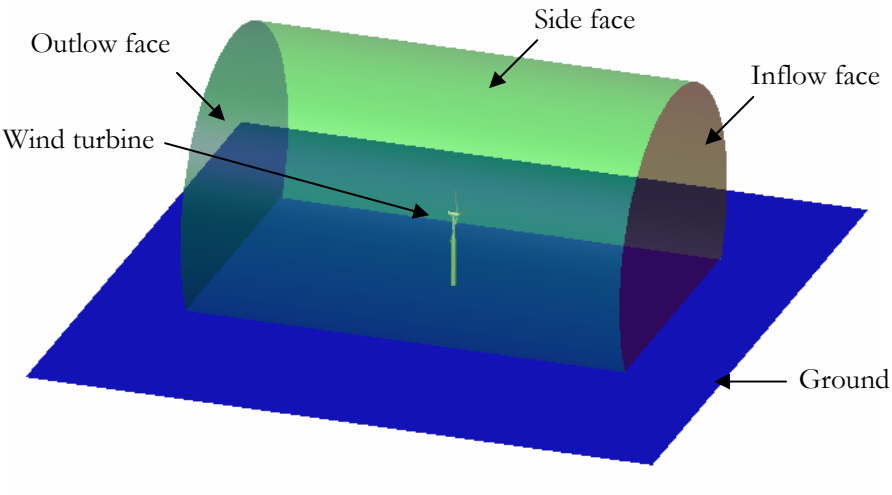

Figure 1: Section of a cylinder control volume, centred on the wind turbine.

This control volume increases the complexity of the equations, as the spatial integration of the wind speed has to take into account the missing section. One way of doing that is to separate the integration in two parts: a slice of the disc, and a triangle (Figure 2).

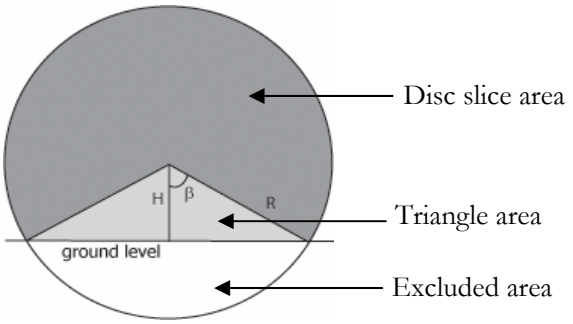

Figure 2: Disc section control surface. The spatial integration is carried on two different parts (the disc slice and the triangle), while the underground section is left over.

The angle of the slice 2β, can be expressed simply as (I-1.1).

$$\beta = ArcCos\left(\frac{H}{R}\right) \tag{I-1.1}$$

And the area of the disc section A_0 (I-1.4), is the sum of the area of the disc slice (I-1.2), and the triangle (I-1.3).

$$A_{Slice} = \int_0^R 2(\pi - \beta) r\, dr = R^2(\pi - \beta) \tag{I-1.2}$$

$$A_{Triangle} = \int_0^H 2r\tan(\beta)\, dr = H\sqrt{R^2 - H^2} \tag{I-1.3}$$

$$\boxed{A_0 = H\sqrt{R^2 - H^2} + R^2(\pi - \beta)} \tag{I-1.4}$$

1.4 No shear forces acting on the control volume

In order to simplify the equations, it can be interesting to drop the shear forces acting on the control volume side face. In order to do so, the control volume must be wide enough to encompass all the shear work done by the atmosphere on the wake area. In that case, this assumption is quite acceptable. It is therefore interesting to relate the width of the control volume with the wake width (i.e. the width of the disturbed flow behind the turbine).

There might still be a problem of realism with the accuracy of this assumption, in the case of a wind farm, or other kind of obstacles creating another wake. In that case, the wake of the turbine might eventually merge with the wake of other wind turbines/obstacles before recovering completely. This would introduce some extra shear forces that cannot be neglected.

1.5 No gravity work

For the sake of simplification, the gravity work acting inside the control volume is neglected. It is difficult to estimate how much uncertainty this assumption will create. However, it is clearly unrealistic to consider that the wake will expend the same way horizontally and vertically. Nonetheless, this assumption is necessary because it is linked with the assumption of axis symmetry presented later on.

1.6 Rectangular inflow profile

The general way of describing a flow in the wind energy domain, is to consider the wind distribution following a logarithmic profile (I-1.5).

$$u(z) = \frac{u^*}{\kappa} \ln\left(\frac{z}{z_0}\right) \tag{I-1.5}$$

Unfortunately, this equation is not axis symmetric and cannot be easily integrated over a disc. For this reason, the inflow profile is taken as rectangular, so without taking into account the influence of the wind shear.

It is usually considered that the inflow wind profile has an important impact on the wake distribution. Consequently, this assumption is quite unrealistic. What could be done to consider the wind shear, is to integrate numerically the wind speed over the control volume. However, this solution would introduce another degree of complexity in the formula, and would require some further assumptions on the vertical wake shape.

1.7 Wake profile

1.7.1 Self similarity

Most of the models of wind turbine wake are based on the assumption of self-similarity, i.e. that the mean velocity flow field becomes self similar for any distance behind the turbine. It also means

that the turbulence generated by Reynolds stress is assumed self-similar. So both the mean and the turbulent field can solely be described by the local scale of length and velocity [Kundu et al., 2002, p.524].

In other words, the velocity field behind the turbine is completely determined by the evolution of the centerline velocity $U_c(x)$, and the scale of the wake $R(x)$, at a distance x from the turbine (I-1.6).

$$U_w(x,y,z) = U_\infty - \left(U_\infty - U_c(x)\right) f\left(\frac{y}{R(x)}, \frac{z}{R(x)}\right) \tag{I-1.6}$$

This assumption is originally used in wall-free flow situations, which is not the case of wind turbines, as the ground presents clearly a physical limit to the evolution of the wake. Furthermore, this assumption presupposes a rectangular inflow profile, which is also untrue, as the wind speed varies with height. Finally, from observation, the horizontal self-similarity at hub height seems to be reached after 6 to 7 rotor diameters, so after the development of the wake when it has finished rotating. Nonetheless, this assumption is the basis of most analytical analysis of the far wake situations.

1.7.2 Rectangular wake profile

In this sub section and the following, two kinds of wake profiles are assumed in order to solve the momentum and energy balance analytically. The simplest one is the rectangular profile, or "top hat" profile that assumes the velocity field to be the same at a given distance from the turbine. This unrealistic assumption simplifies greatly the integrations, but, is not appropriate to compare the theory with measurements.

1.7.3 Axis symmetric wake profile

In order to go a little bit further, the wake profile can be assumed axis symmetric. For a given distance from the turbine, the velocity field is assumed to have an axis symmetry relative to the centerline in comparison with the wake scale R.

$$U_w(x,r) = U_\infty - \left(U_\infty - U_c(x)\right) f\left(\frac{r}{R(x)}\right) \tag{I-1.7}$$

As it was suggested by Ainslie [1988], a normal distribution is found to be an appropriate description of an axis symmetric wake. The function f can then be defined as (I-1.8), where ζ is the radial position scaled over the wake width, and k an empirical shape factor.

$$f_k(\zeta) = e^{-k\zeta^2} \tag{I-1.8}$$

This wake shape can be integrated over the disc section of the control volume, presented in section 1.3 (Figure 2), in order to derive the wind speed spatial average over the inflow/outflow surface. Similarly for the area derivation method, the disc section can be separated into two areas, the triangle and the disc slice (I-1.9), with R the wake width, and H the hub height.

$$\overline{f_k}(x) = \frac{1}{A_0}\int_{A_0} f_k\left(\frac{r}{R(x)}\right) = \frac{1}{A_0}\left(\int_0^H 2e^{-k\left(\frac{r}{R_x}\right)^2} \tan(\beta) r\, dr + \int_0^{R(x)} 2(\pi-\beta) e^{-k\left(\frac{r}{R(x)}\right)^2} r\, dr\right) \tag{I-1.9}$$

$$\overline{f_k}(x)=\frac{R^2(x)}{k\,A_0(x)}\left[\left(1-e^{-k\left(\frac{H}{R(x)}\right)^2}\right)\frac{\sqrt{R^2(x)-H^2}}{H}+\left(\pi-\beta(x)\right)\left(1-e^{-k}\right)e^{-k}\right] \tag{I-1.10}$$

By substituting $H \to R(x)\cdot\eta(x)$, where $\eta(x)$ is a non dimensional parameter relating the wake expansion with the hub height, and using (I-1.4) the expression can be simplified to (I-1.11).

$$\boxed{\overline{f_k}(x)=\frac{1}{k\eta(x)}\frac{\left(1-e^{-k\eta^2(x)}\right)\sqrt{1-\eta^2(x)}+\eta(x)\left(1-e^{-k}\right)\left(\pi-\beta(x)\right)}{\eta(x)\sqrt{1-\eta^2(x)}+\left(\pi-\beta(x)\right)}} \tag{I-1.11}$$

At some point, it becomes necessary to integrate the square of the wake shape. In those cases, it is interesting to note the following property of the equation (I-1.11). Because of the lack of symmetry of the disc section, the integration of the square of the wake shape is not the same as the square of the integration of the wake shape. However, it is the same as the integration of the wake shape with a parameter *2 k* (I-1.12).

$$\boxed{\begin{cases}\overline{f_k^2}=\overline{f_{2k}}\neq\overline{f_k}^2\\ \overline{f_k^n}=\overline{f_{nk}}\neq\overline{f_k}^n,\ \forall n\in\mathbb{N}\end{cases}} \tag{I-1.12}$$

2 Momentum balance

In this section, the thrust coefficient and the centerline deficit is derived using the law of conservation of momentum over a wind turbine system defined under the assumptions introduced in the previous section. These results can be used as a method, presented in Chapter III, to estimate the thrust coefficient of a turbine using wake wind speed measurements.

2.1 Thrust equation

2.1.1 Integrated over the control volume

The thrust, or more generally the drag force of an object, is related to the surrounding flow characterized by the momentum theory. This theory is based on the second Newton's law, which relates the motion of the system with the forces applied on it and is an integral form derived from the Navier-Stokes equations [White, 2001, p.146]. In the present case of a wind turbine, the system is taken as a control volume surrounding the turbine. In order to simplify the calculations, the control volume characterizing the system will be taken as a section of a cylinder encompassing the turbine such as pictured in Figure 1, where the inflow face and the outflow face have the same area.

The momentum theory applied to a control volume states that the total sum of the forces acting on the control surface (CS) and inside the control volume (CV) of the system must be equal to the

change of momentum going through the control volume and the time variation of mass flow inside the control volume.

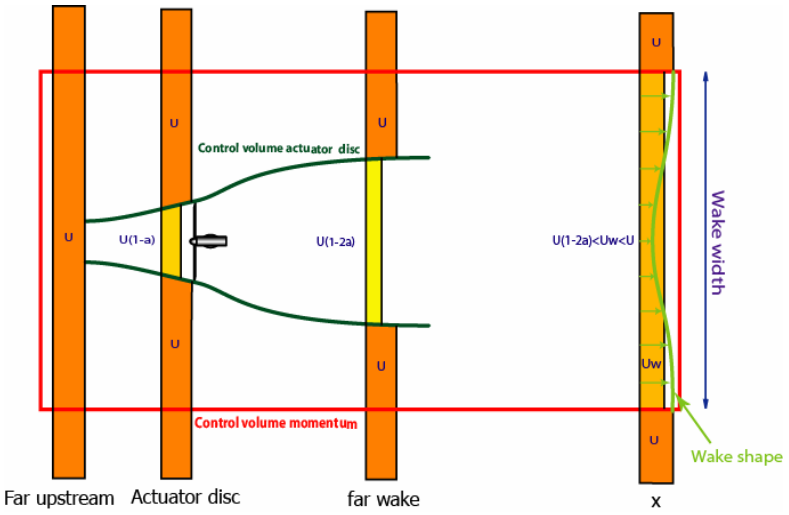

Figure 3: Illustration of the two control volumes (actuator disc and linear momentum theory)

In equation (I-2.1), the total expression of the forces can be represented by the thrust of the turbine *T*, the pressure forces acting on the control surface *p*, the gravity forces *g* and the shear forces on the control surface τ [Frandsen, 2005, p.121].

$$\vec{T} - \int_{CS} p\,\overrightarrow{dA} + \int_{CV} \rho \vec{g}\, dV + \int_{CS} \vec{\tau}\, dA = \frac{d}{dt}\left(\int_{CV} \rho \vec{U}\, dV\right) + \int_{CS} \rho \vec{U}\left(\vec{U} \cdot \overrightarrow{dA}\right) \tag{I-2.1}$$

Equation (I-2.1) can be simplified using the previously defined assumptions. In steady flow condition, the acceleration term can be neglected, as the flow is considered independent of time. If the control surface is symmetrical around the wind turbine, and the system is assumed to be axis symmetric, the gravity term can also be neglected. In addition, by taking the control volume far enough from the turbine to neglect the shear forces on the surface, and the pressure difference, the momentum equation is simplified to (I-2.2).

$$\vec{T} = \int_{CS} \rho \vec{U}\left(\vec{U} \cdot \overrightarrow{dA}\right) \tag{I-2.2}$$

If the thrust vector is assumed parallel with the inflow velocity vector, the problem can be reduced to one dimension. The thrust is then equal to the difference between the inflow momentum $\dot{M}_{in}$ and the outflow momentum through the side face $\dot{M}_{side}$ and the outflow face $\dot{M}_{out}$ [Kundu, 2001, p.91].

$$T = -\dot{M}_{in} + \dot{M}_{out} + \dot{M}_{side} \tag{I-2.3}$$

The momentum going through the inflow and outflow faces can be derived using the inflow wind distribution U_∞, and the outflow wind distribution U_w.

$$\dot{M}_{in} = \int_{A_0} \rho U_\infty^2\, dA \tag{I-2.4}$$

$$\dot{M}_{out} = \int_{A_w} \rho U_w^2\, dA \tag{I-2.5}$$

It is important to keep in mind that there is necessarily an outflow going through the side face. If the inflow face and the outflow face have the same area ($A_0 = A_w$), by using the conservation of mass, and multiplying the massflow expression (I-2.6) by the free stream wind speed, the rate of momentum through the side face can be expressed as (I-2.7).

$$\dot{m}_{side} = \dot{m}_{in} - \dot{m}_{out} = \int_{A_0} \rho \left(U_\infty - U_w \right) dA \tag{I-2.6}$$

$$\dot{M}_{side} = U_\infty \dot{m}_{side} = \int_{A_0} \rho U_\infty \left(U_\infty - U_w \right) dA \tag{I-2.7}$$

Which leads to the final expression of the wind turbine thrust (I-2.8) [Kundu, 2001, p.91; and Frandsen, 2005, p.122].

$$T = -\int_{A0} \rho U_w \left(U_\infty - U_w \right) dA \tag{I-2.8}$$

2.1.2 Using a rectangular wake profile

In order to express the wind speed deficit downstream the turbine using the thrust coefficient, further approximations must be done. By assuming a rectangular wind speed distribution of both the inflow wind speed U_∞ and the wake wind speed U_w, the integration of equation (I-2.8) becomes straight forward [Frandsen, 2005, p.122].

$$T = -\rho A_w U_w \left(U_\infty - U_w \right) \tag{I-2.9}$$

By combining the equation (I-2.9) with the definition of the thrust coefficient C_T (I-2.10), where A_T is the rotor disc area; the thrust coefficient can be expressed as (I-2.11).

$$C_T = -\frac{T}{½ \rho A_T U_\infty^2} \tag{I-2.10}$$

$$C_T = 2 \frac{A_w}{A_T} \left(1 - \frac{U_w}{U_\infty} \right) \frac{U_w}{U_\infty} \tag{I-2.11}$$

2.1.3 Using an axis symmetric wake profile

If the assumption of an axis symmetric normal distribution is used instead of the rectangular wake profile, it becomes necessary to introduce the wake shape parameter in order to solve the integral (I-2.8). Indeed, equation (I-2.8) can be directly derived as equation (I-2.12), which shows that, with a rectangular inflow assumption, the integral can be split into two integrals of the spatial average of the wind speed and, the wind speed squared.

$$T = -\int_{A0} \rho U_\infty U_w \, dA + \int_{A0} \rho U_w^2 \, dA = \rho A_w \overline{U_w^2} - \rho A_w U_\infty \overline{U_w} \tag{I-2.12}$$

Under the self-similarity assumption of the wake profile, the wind speed behind the wind turbine can be expressed independently from the distance from the turbine. This is done in equation (I-2.13), x is the distance behind the turbine, r is the distance from the wake centerline, where the wake deficit is maximum, and $R_w(x)$ is the wake width, a parameter which quantify the radial expansion of the wake.

$$\boxed{U_w(x,r) = U_\infty - \left(U_\infty - U_{\min}(x) \right) f\left(\frac{r}{R_w(x)} \right)} \tag{I-2.13}$$

In that case, the spatial average of $\overline{U_w}$ and $\overline{U_w^2}$ can be derived as equations (I-2.14).

$$\begin{cases} \overline{U_w} = U_\infty - \left(U_\infty - U_{\min}\right)\overline{f} \\ \overline{U_w^2} = U_\infty^2 + \left(2U_\infty U_{\min} - 2U_\infty^2\right)\overline{f} + \left(U_\infty^2 - 2U_\infty U_{\min} + U_{\min}^2\right)\overline{f^2} \end{cases} \quad \text{(I-2.14)}$$

In order to simplify the formulations, the relative wind speed is defined as (I-2.15)

$$\delta_X = \frac{U_\infty - U_X}{U_\infty} \quad \text{(I-2.15)}$$

Which has the nice property of being spatially integrated more easily (I-2.16).

$$\begin{cases} \overline{\delta_w} = \delta_{\min}\,\overline{f} \\ \overline{\delta_w^2} = \delta_{\min}^2\,\overline{f^2} \end{cases} \quad \text{(I-2.16)}$$

Using this notation, the wake profile can be express as (I-2.17)

$$\boxed{U_w\left(x,r\right) = U_\infty\left[1 - \delta_{\min}\left(x\right) f\left(\frac{r}{R_w\left(x\right)}\right)\right]} \quad \text{(I-2.17)}$$

And its spatial integration can be express as (I-2.18)

$$\boxed{\begin{cases} \overline{U_w} = U_\infty\left[1 - \delta_{\min}\,\overline{f}\right] \\ \overline{U_w^2} = U_\infty^2\left[1 - 2\delta_{\min}\,\overline{f} + \delta_{\min}^2\,\overline{f^2}\right] \\ \overline{U_w^3} = U_\infty^3\left[1 - 3\delta_{\min}\,\overline{f} + 3\delta_{\min}^2\,\overline{f^2} - \delta_{\min}^3\,\overline{f^3}\right] \end{cases}} \quad \text{(I-2.18)}$$

Combined into equation (I-2.12), the thrust, under the assumption of self similarity of the wake, becomes (I-2.19).

$$\boxed{T = -\rho A_w U_\infty^2\left(\overline{f} - \delta_{\min}\,\overline{f^2}\right)\delta_{\min}} \quad \text{(I-2.19)}$$

With the definition of the thrust coefficient previously defined as (I-2.10), the thrust coefficient can be simplified to (I-2.20)

$$\boxed{C_T = 2\,\frac{A_w}{A_T}\left(\overline{f} - \delta_{\min}\,\overline{f^2}\right)\delta_{\min}} \quad \text{(I-2.20)}$$

So, as with the rectangular wake profile assumption, the thrust coefficient is related only with the wake width and the centerline wind speed deficit.

2.2 Wake wind speed distribution

If the thrust coefficient is known, and the unknowns are the wake parameters, the problem can be taken in the opposite direction to derive the centerline wind speed deficit with respect to the wake width.

2.2.1 Using a rectangular wake profile

By combining the equation (I-2.9) with the definition of the thrust coefficient (I-2.10), where A_T is the rotor disc area, and C_T is the trust coefficient; the wake wind speed U_w has two solutions (I-2.21) [Frandsen, 2005, p.93].

$$U_w = \frac{U_\infty}{2}\left(1 \pm \sqrt{1 - 2C_T \frac{A_T}{A_w}}\right) \tag{I-2.21}$$

As it can be seen on Figure 4, only the solution with the '+' makes sense, as the ratio U_w/U_∞ is expected to increase until it reaches 1 for an increasing control volume width. As the effect of the turbine will have a decreasing effect on the flow.

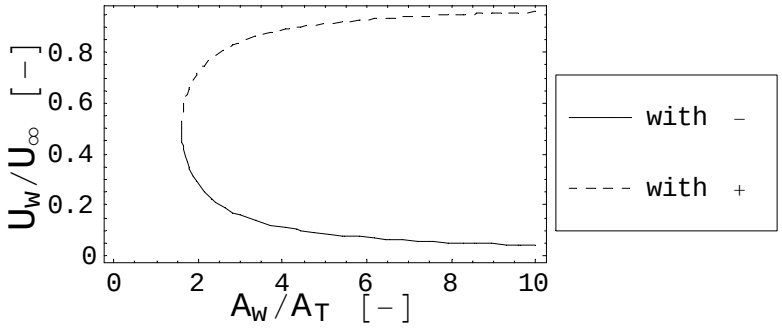

Figure 4 The average wake wind speed ratio with respect to the size of the control volume considered (C_T=0.8)

The final solution for a rectangular wake profile is therefore found to be

$$U_w = \frac{U_\infty}{2}\left(1 + \sqrt{1 - 2\frac{A_T}{A_w}C_T}\right) \tag{I-2.22}$$

2.2.2 Using an axis symmetric wake profile

Similarly, the solutions for a self similar wake profile is derived using (I-2.20).

$$\delta_{\min} = \frac{1}{2}\frac{\overline{f}}{\overline{f^2}}\left(1 \pm \sqrt{1 - 2\frac{\overline{f^2}}{\overline{f}^2}\frac{A_T}{A_w}C_T}\right) \tag{I-2.23}$$

Using a normal distribution for the wake shape, as defined previously, the 2 solutions can be plotted with respect to the relative increase of the wake width from the rotor diameter.

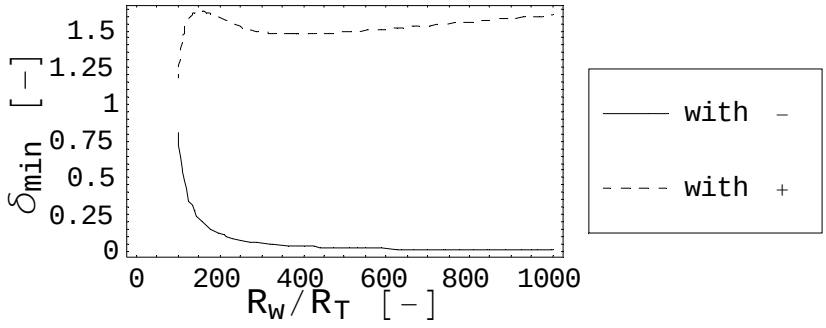

Figure 5 Relative difference of the minimum wake wind speed with respect to the relative increase of wake width, using a normal axis symmetric self similar wake profile (C_T=0.8)

The relative difference of centerline wake wind speed is expected to decrease as the wake width is increasing. Consequently, the final solution is the one with a minus.

$$\delta_{\min} = \frac{1}{2}\frac{\overline{f}}{\overline{f^2}}\left(1-\sqrt{1-2\frac{\overline{f^2}}{\overline{f}^2}\frac{A_T}{A_w}C_T}\right) \qquad \text{(I-2.24)}$$

It is quite interesting to note that under these assumptions, if the wake shape is known, the wind speed distribution behind the turbine depends only of the thrust coefficient and the rotor disc area. In this system, there are two main unknowns, the wake width, and the centerline wind speed deficit. Equation (I-2.24) gives one relation between those two. However, another equation is needed in order to close completely the problem. The equation of motion could be used to close this system, but the second order derivative terms are difficult to adapt to this analytical method. Nonetheless, this means that this system can be solved numerically using CFD methods.

3 Energy balance

The momentum balance is used in the previous section to derive the expression of the thrust coefficient from the inflow and outflow wind characteristics. A similar approach can be used to express the kinetic power lost by the flow through the work of the wind turbine.

3.1 Integrated over the control volume

The law of conservation of energy is built similarly to the momentum theory, as they can both be derived from the Reynolds transport theorem [White, 2001, p.164].

$$\dot{Q}+\dot{W}_{shaft}+\dot{W}_{press}+\dot{W}_{viscous\ stresses}=\frac{d}{dt}\left(\int_{CV}\left(\hat{u}+\frac{1}{2}U^2+gz\right)\rho\,dV\right)+\int_{CS}\left(\hat{u}+\frac{1}{2}U^2+gz\right)\rho\left(\vec{U}\cdot\vec{dA}\right) \qquad \text{(I-3.1)}$$

The energy term is constituted of the internal energy $\hat{u}$ (e.g. heat), the kinetic energy $\frac{1}{2}U^2$, and the potential energy gz. There is no heat added to the system externally, and no work of the pressure forces or of the viscous stresses on the control surface (assuming that the control volume

is taken at a radial distance far enough from the turbine). It remains therefore only the power consumed by the work done on/by the shaft

Under the assumption of steady process, the first term of the right hand side can be dropped, as there is no variable dependant of the time. If the potential energy term is neglected and the internal energy termed are gathered into a term P_{Heat} , quantifying the amount of power consumed as heat, equation (I-3.1) is reduced to (I-3.2), where the term P_{Ext} refers to the amount of power extracted by the turbine [Frandsen, 2005, p.122].

$$P_{Ext} + P_{Heat} = \int_{CS} \frac{1}{2} U^2 \, \rho\left(\vec{U} \cdot \overrightarrow{dA}\right) \tag{I-3.2}$$

Following the same method as with the derivation of the thrust, equation (I-3.2) can be derived on the control volume.

$$P_{Ext} + P_{Heat} = -\dot{E}_{in} + \dot{E}_{out} + \dot{E}_{side} \tag{I-3.3}$$

with

$$\begin{cases} \dot{E}_{in} = \int_{A_0} \frac{1}{2} \rho U_\infty^3 \, dA \\ \dot{E}_{out} = \int_{A_0} \frac{1}{2} \rho U_w^3 \, dA \\ \dot{E}_{side} = \int_{A_0} \frac{1}{2} \rho U_\infty^2 \left(U_\infty - U_w\right) dA \end{cases} \tag{I-3.4}$$

Combined together, the final expression of the extracted power and heat power becomes (I-3.5) [Frandsen, 2005, p.122].

$$P_{Ext} + P_{Heat} = -\int_{A_0} \frac{1}{2} \rho U_w \left(U_\infty^2 - U_w^2\right) dA \tag{I-3.5}$$

3.2 Using a rectangular wake profile

Under the rectangular wake profile assumption the integral of (I-3.5) becomes straight forward Frandsen, 2005, p.122].

$$P_{Ext} + P_{Heat} = -\frac{1}{2} \rho A_w U_w \left(U_\infty^2 - U_w^2\right) \tag{I-3.6}$$

Using the expression of the wake wind speed for a rectangular wake profile derived previously (I-2.22), the total extracted power and power converted as heat in the control volume can be expressed as a function of the thrust coefficient C_T (I-3.7).

$$\boxed{P_{Ext} + P_{Heat} = -\frac{1}{8} \rho A_T C_T \left(3 + \sqrt{1 - 2\frac{A_T}{A_w} C_T}\right) U_\infty^3} \tag{I-3.7}$$

3.3 Using self similar wake profile

Similarly as for momentum theory, the spatial average of the wake wind speed is not linear, and $\overline{U_w}^3 \neq \overline{U_w^3}$.

$$P_{Ext} + P_{Heat} = -\frac{1}{2}\rho U_\infty^2 \int_{A_w} U_w \, dA + \frac{1}{2}\rho \int_{A_w} U_w^3 \, dA = -\frac{1}{2}\rho A_w \left(U_\infty^2 \overline{U_w} - \overline{U_w^3} \right) \tag{I-3.8}$$

The relative wind speed can be used to simplify the integration of the total extracted power. Using equation (I-3.8) and (I-2.18), equation (I-3.8) can be reduced to (I-3.9).

$$\boxed{P_{Ext} + P_{Heat} = -\frac{1}{2}\rho A_w U_\infty^3 \left(\delta_{\min} \overline{f} - 3\delta_{\min}^2 \overline{f^2} + \delta_{\min}^3 \overline{f^3} \right)} \tag{I-3.9}$$

Using the expression of the relative wind speed found with the conservation of momentum (I-2.24), the total extracted power can be expressed as a function of the thrust coefficient, the wake shape, the rotor area and the inflow control surface area (I-3.10). This expression can be solved and simplified in the software *Mathematica* but remains too complex to be presented here.

$$P_{Ext} + P_{Heat} = -\frac{1}{2}\rho U_\infty^3 \, \Phi\left(A_T, A_w, f, C_T \right) \tag{I-3.10}$$

Chapter II
Importance of the thrust accuracy

Using the theory described in Chapter I and Appendix A, it is possible to relate the thrust coefficient and the power coefficient with the properties of the flow in the wake of a turbine. The current models describing the wind speed deficit inside large wind turbine clusters are based on a similar approach [Frandsen, 2005, p.121; Vermeer et al. 2003]. Consequently, most of these models are largely relying on the thrust coefficient of the turbine given by the manufacturer. In the majority of the cases, the thrust coefficient curves publicly available are determined using a Blade Element Method simulating the wind turbine. These BEM codes are usually optimized using empirical methods to simulate with accuracy the real power output and the blade loading of the turbines. However, the validity and accuracy of the thrust is not always analyzed.

In this Chapter, the results derived from Chapter I and Appendix A are used to stress the importance of having an accurate knowledge of the thrust of a wind turbine. Firstly, using the method to derive the combined uncertainty, presented in Appendix B, the sensitivity coefficient of the thrust coefficient contributing to the uncertainty of the wake wind speed is derived and briefly analyzed. The significant result of this section is that, in the worst-case scenario, the uncertainty of the thrust coefficient is directly propagated to the wake wind speed with a sensitivity coefficient of 100%. A 10% inaccuracy of the thrust coefficient would yield an equivalent 10% inaccuracy in the centerline wake wind speed.

Secondly, a pragmatic approach is used to show the relationship between the thrust force applied on the rotor and the amount of turbulent kinetic power generated by the turbine. A brief application is done on two different types of wind turbines (Pitch and active stall regulated). However, further work needs to be done on this subject to be able to fully relate the wake turbulent field with the thrust coefficient.

1 Importance for estimating the wake wind speed

If the thrust coefficient is known, the uncertainty in wind speed deficit behind a turbine is derived easily from equation (II-1.1), which is derived from the momentum conservation in Chapter I - 2.2.2 .

$$\boxed{\delta_{\min} = \frac{1}{2}\frac{\overline{f}}{\overline{f^2}}\left(1-\sqrt{1-2\frac{\overline{f^2}}{\overline{f}^2}\frac{A_T}{A_w}C_T}\right)} \qquad \text{(II-1.1)}$$

With f a wake shape parameter, which is presented in section Chapter I - 1.7.3 , and is defined as

$$\boxed{\overline{f_k} = \frac{\left(1-e^{-k\eta^2}\right)\sqrt{1-\eta^2}+\eta\left(1-e^{-k}\right)(\pi-\beta)}{k\eta^2\sqrt{1-\eta^2}+k\eta(\pi-\beta)}} \qquad \text{(II-1.2)}$$

With k a wake shape factor and $\eta = H_{Hub} / R_{wakewidth}$ the ratio between the hub height and the wake width.

The wake width can be estimated using a semi empirical formula taking into account the thrust coefficient and the axial distance from the turbine. An example is proposed by Frandsen [2005, p.93] based on similar assumptions (self-similarity of the turbulent and mean flow field) (II-1.3).

$$D(x) = D_{Rotor}\left(\beta^{\kappa/2} + \alpha\frac{x}{D_{Rotor}}\right)^{1/\kappa} \tag{II-1.3}$$

Where $\kappa \approx 2 or 3$ is an empirical value, β is a value relating the wind turbine rotor area with the initial expansion of the wake predicted by the actuator disc theory $D_{wake} = \sqrt{\beta} D_{Rotor}$, derived easily from the relationship between the induced velocity and the thrust coefficient (II-1.4), and α is a variable determined experimentally, which can also depend of the thrust coefficient.

$$\beta = \frac{1+\sqrt{1-C_T}}{2\sqrt{1-C_T}} \tag{II-1.4}$$

The derivation of the uncertainty in wind speed deficit follows the same rule presented in the Appendix B. It is the root sum square of the standard uncertainty of each element of equation (II-1.1) multiplied by a sensitivity coefficient obtained with the partial derivative of equation (II-1.1) with respect to the element considered. The standard uncertainty of the thrust coefficient is therefore used both for the wake width expansion formula and for the thrust coefficient itself. The final formula is extremely complicated, and represents little interest for the present report. However, the formula is fully solvable using symbolic math software like *Mathematica* and can also be solved numerically.

A concrete example is proposed to apply this theory. In the case of a generic pitch regulated 2MW turbine with a rotor diameter of 80m, an hub height of 60m, at 7 rotor diameters downstream with a flow expansion parameter $\alpha = 0.5$, a thrust coefficient of 0.7, the uncertainty on the centerline wind speed (i.e. the minimum wind speed in full wake effect) is estimated to be (II-1.5). Therefore, under these conditions, any uncertainty on the thrust coefficient will be almost identically propagated to the uncertainty of wind speed.

$$\boxed{u_c(U_{\min}) \approx 1.06 \cdot U_\infty \cdot u(C_T)} \tag{II-1.5}$$

This represents, however, the worst-case scenario, and in general, the sensitivity coefficient is between 30%-100%. Figure 6, Figure 7 and Figure 8 present the distribution of the sensitivity coefficient for a similar turbine, with various thrust coefficient and flow expansion factors. For lower values than $\alpha < 0.5$, the uncertainty parameter is undefined in some occasion because the wake width is smaller than the hub height, and the previous equations are not valid. However after seven rotor diameters, the wake width is, in general, much larger than the hub height.

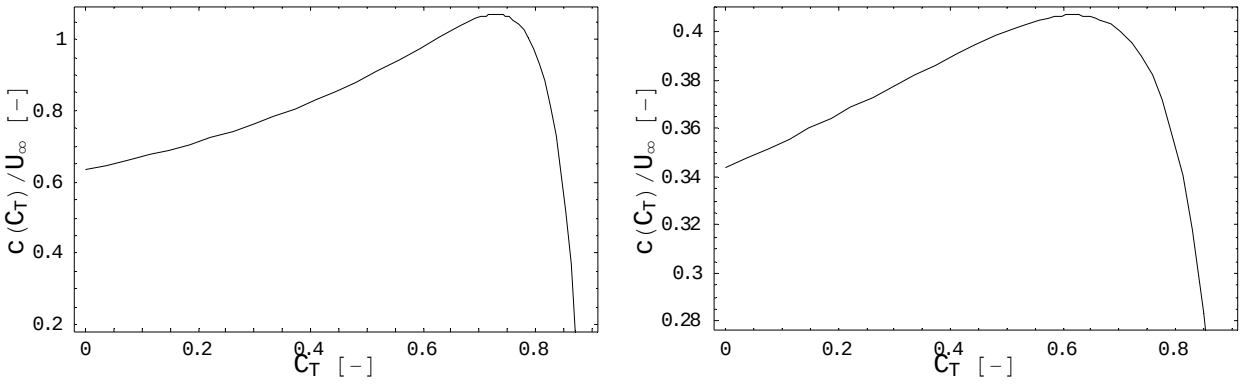

Figure 6: Evolution of the thrust coefficient sensitivity coefficient with respect to the thrust coefficient, with a flow expansion parameter $\alpha = 0.5$ (left) and $\alpha = 1$ (right).

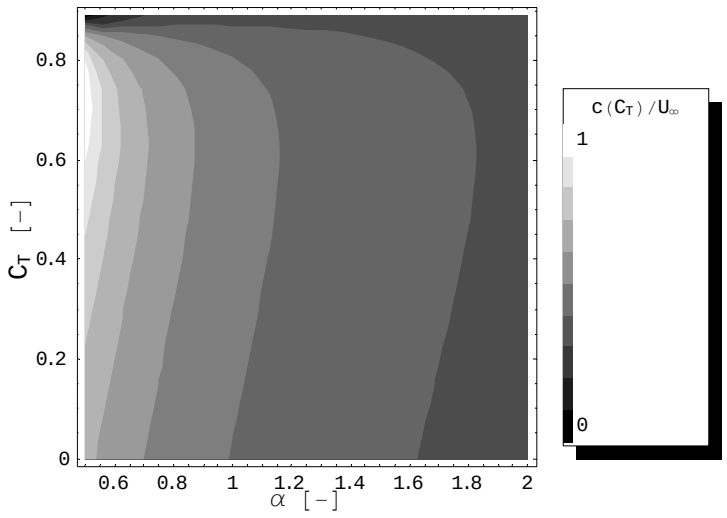

Figure 7: Evolution of the thrust coefficient sensitivity coefficient with respect to the thrust coefficient C_T and the flow expansion parameter α .

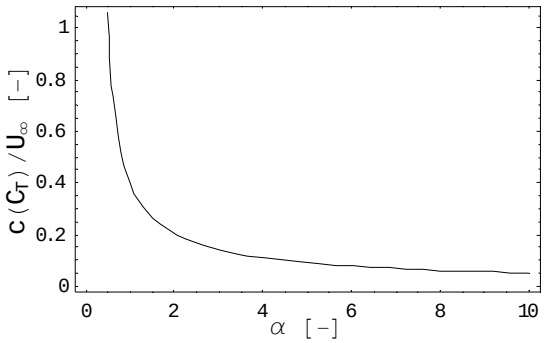

Figure 8: Evolution of the thrust coefficient sensitivity coefficient for an increasing wake expansion factor α , with $C_T = 0.7$.

While this application is intentionally reductive, by using more advanced semi empirical rules in a similar manner, the standard uncertainty of the mean flow field can be estimated inside a wind farm. Therefore, they can also be used to quantify the uncertainty of the power produced by each wind turbine, and ultimately the uncertainty in Annual Energy Production of a wind farm.

2 Importance for estimating the wake turbulence

The wind turbines wake turbulence is widely considered as an important source of fatigue in wind turbine clusters. The IEC standards [IEC61400-12, 2003] are proposing an engineering rule to estimate the fatigue of the wind turbines in cluster taking as an input the thrust coefficient of the turbines. The model behind this rule, developed by Frandsen [2005], is based on the simplified geostrophic drag law, considering the atmospheric boundary layer in equilibrium with the roughness generated by the wind turbines thrust. So any uncertainty of the thrust coefficient can be in theory propagated to an uncertainty of the wake turbulence seen felt by turbines in cluster, and ultimately to an uncertainty on the operational fatigue of the turbines and an uncertainty over their lifetime.

While this theory is out of the scale of this thesis, it is possible to relate the amount of turbulence generated by a turbine with the thrust coefficient using the conservation of energy presented in Chapter I.

2.1 Relationship between the thrust and the wake turbulence

In equation (I-3.7), in Chapter I, the total extracted power by the turbine is given as a relationship between the disc area, the rotor area, the inflow wind speed and the thrust coefficient (II-2.1). This extracted power represents the amount of power needed by the flow going through the control volume to recover from the presence and the work of the turbine. It is a general formula that can be applied to any bluff body with a drag coefficient C_T, and a sectional area A_T, inside a flow of velocity U_∞.

$$\boxed{P_{Ext} + P_{Heat} = -\frac{1}{8}\rho A_T C_T \left(3 + \sqrt{1 - 2\frac{A_T}{A_w} C_T}\right) U_\infty^3} \quad \text{(II-2.1)}$$

As the control volume is increased, more particles of the flow are disturbed by the work of the turbine, and therefore more kinetic energy is "lost" as heat through the mixing in the wake. By making the width of the cylindrical control volume tend to infinity, the whole system wind / turbine is taken into account, and the total power needed by the flow to recover from the work of the turbine can be found (II-2.2).

$$\boxed{\lim_{A_w \to \infty} P_{Ext} + P_{Heat} = \frac{1}{2}\rho A_T C_T U_\infty^3} \quad \text{(II-2.2)}$$

Corten [2001] presented also, in is PhD thesis, a similar result based on an extension of the actuator disc theory.

This finding is not in contradiction with the actuator disc theory, and the Betz limit, which says that only 59% of the energy contained in the flow going through the rotor can be extracted. The energy "lost" cannot be extracted as it is used by the flow to recover from the turbine work.

This is the same kind of problem than putting a wind turbine on a car and driving it through an immobile flow: the amount of power used to drive the car is representing the maximum amount of power available for extraction. However, because of the Betz law, the turbine can only extract a part of this power. The remaining of the power of the car, which is equal to the sum of the forces applied on it multiplied by its speed is lost as heat through the generation of shear turbulence.

In fact, Glauert mentioned this loss of energy in the establishment of his general momentum theory of propellers [Glauert, 1935, p.196].

$$V\left(1+a\right)dT = \Omega\left(1-a'\right)dQ$$

This relationship, valid for a propeller, is equivalent to

$$\Omega dQ - VdT = VadT + \Omega a'dQ$$

"*The left hand side represents the excess of the power absorbed by the propeller over the useful work done by the thrust, and the right hand side is an expression for the work done on the air or for the loss of energy.*"

In the context of a wind turbine, the left hand side is of opposite sign: the generated mechanical power is equal to the rotation speed of the rotor multiplied by the rotor torque, and the power absorbed by the turbine is equal to the velocity of the flow multiplied by the useful work of the turbine. The left hand side remains the same. The corresponding formula becomes:

$$V\left(1-a\right)dT = \Omega\left(1+a'\right)dQ$$

is equivalent to

$$\boxed{V\,dT - \Omega\,dQ = V\,a\,dT + \Omega\,a'dQ}$$

Therefore, the difference between the useful work done by the thrust on the flow, and the power transformed into mechanical power is equal to the work done on the air, in another word, the additional loss of energy. The second term of the right hand side accounts for the rotation of the wake and the first term of the right hand side accounts for the energy causing the mixing as well as other energy losses.

Part of the energy lost by the flow is gone through the turbulence generated by the turbine, and by the work of shear forces of the flow acting in the wake. It is therefore of interest to analyze how much energy is contained in those turbulence.

The losses in kinetic energy of the flow can be divided into three parts. The first part is the energy converted into electricity, the second part is referred as the initial loss of kinetic energy, and the third part is referred as the wake mixing losses.

$$\boxed{P_{tot} = P_{elec} + P_{lost\,init} + P_{lost\,mixing}} \qquad \text{(II-2.3)}$$

This equation (II-2.3) can also be expressed using non dimensional coefficients (II-2.4).

$$C_T = C_{P\,elec} + C_{P\,lost\,init} + C_{P\,lost\,mixing} \qquad \text{(II-2.4)}$$

2.2 Initial losses

The initial losses of kinetic energy (II-2.6) are the losses predicted by the actuator disc theory: computed from the difference between the real power coefficient measured by the power output of the turbine, and the theoretical power coefficient computed through the thrust coefficient formula (III-4.12) presented in Appendix A. This formula (II-2.5), derived from the actuator disc theory, relates the thrust with the energy extracted by the actuator disc, i.e. the electrical energy, and the initial losses.

$$C_{P\,actuator} = C_{P\,elec} + C_{P\,lost\,init} = \frac{1}{2}\left(1+\sqrt{1-C_T}\right)C_T \tag{II-2.5}$$

$$\boxed{C_{P\,lost\,init} = \frac{1}{2}\left(1+\sqrt{1-C_T}\right)C_T - C_{P\,elec}} \tag{II-2.6}$$

The electrical power coefficient can be derived using a well-calibrated blade element code with empirical corrections. It can also be directly measured from the power output of the turbine.

The initial losses are coming from various sources:

- The mechanical losses inside the gearbox, the generator, or the structural vibrations of the wind turbine.
- The electrical losses inside the generator and the converters.
- The friction losses of the flow on the structure, directly transformed as heat.
- The turbulent kinetic energy contained in the wake and created by the wake rotation, the detachment of the flow on the blade, the drag of the hub, blades and the tower, and the blades tip and root vortices.

If each of these losses can be quantified, the turbulence initially generated by the turbine (predicted by the actuator disc theory) can be related to the thrust coefficient and the power coefficient with equation (II-2.6).

2.3 Mixing losses

The wake mixing losses can be derived by doing the difference between the C_P expected from the actuator disc theory, and the measured C_T, which is the total kinetic power coefficient lost by the flow (II-2.7).

$$\boxed{C_{P\,lost\,mixing} = \frac{1}{2}\left(1-\sqrt{1-C_T}\right)C_T} \tag{II-2.7}$$

It is assumed that the energy that is not directly "lost" from the flow inside the actuator disc theory control volume (Bottle shape) is lost during the recovery of the wake as a viscous mixing process by transforming the kinetic energy into heat. It is arguable if this energy is lost by the flow passing through the rotor (which therefore limits the amount of energy that can be extracted from

the flow), or by the undisturbed atmospheric flow outside the control volume. This question is not relevant with the current issue, which is to consider the total losses of the flow created by the turbine.

The wake recovery process is done through the work of the shear forces created by the difference of velocity in the flow. This process also generates turbulence, which facilitates the mixing. The energy necessary to generate this turbulence is therefore drawn from the work of the shear forces [Mutlu Summer, 2006, p.14] and should eventually be equal to the extra kinetic energy lost by the flow. This assumption makes sense with the general idea that the energy used to create the flow fluctuations downstream a propeller, a car or even a boat must be drawn from the their own energy. In the case of a turbine, that collects energy instead of spending it, this energy contained in the fluctuations downstream the turbine is a necessary loss of energy that cannot be collected by the turbine.

The wake of the turbine expands gradually as the distance from the turbine increases, this expansion is not an increase of the volume encompassing the disturbed flow/particles but an increase of the amount/number of flow/particles disturbed. The area of the disturbed flow can be used as the outflow face of the control volume used in the conservation of energy presented in section Chapter I. Using this control volume, the amount of kinetic energy lost by the system should be equal to the initial loss of kinetic energy predicted by the actuator disc, and the energy lost – or in the process to be lost – through turbulence. If this assumption is correct, the expansion of the wake and the thrust coefficient are related to the amount of turbulence generated by the shear forces of the flow with equation (II-2.1).

This shear generated turbulence is coming "on top" of the turbulence directly generated by the turbine and the inflow turbulence. If then, the rate of the turbulence dissipation and dispersion can be related to the wake width, the turbulent kinetic energy budget is known at any distance behind the turbine. Unfortunately, very little information could be gathered on this matter, and as the knowledge of the author on this subject is sadly rather limited, it was decided that the current study would not go any further in that direction.

2.4 Simple application to a pitch and an active stall regulated turbine

Therefore, just by using the C_P and the C_T curves given by the wind turbines manufacturers, the two power losses can be directly estimated (Figure 9).

It is quite interesting to notice that the "mixing losses" are decreased for high wind speed after that the turbine has reached its rated power. This makes sense because, if the thrust decrease, the wind speed deficit ratio created by the turbine also decreases when the inflow wind speed increases. Therefore, the amount of kinetic power needed to recover should decrease. On the other hand, the initial losses, which encompass the mechanical and electrical losses as well as the direct turbulence, reach an almost constant level at high wind speed. This is expected as the electrical losses are proportional to the electrical power, and the drag losses (which generate the initial turbulence) are kept constant by pitching the blades.

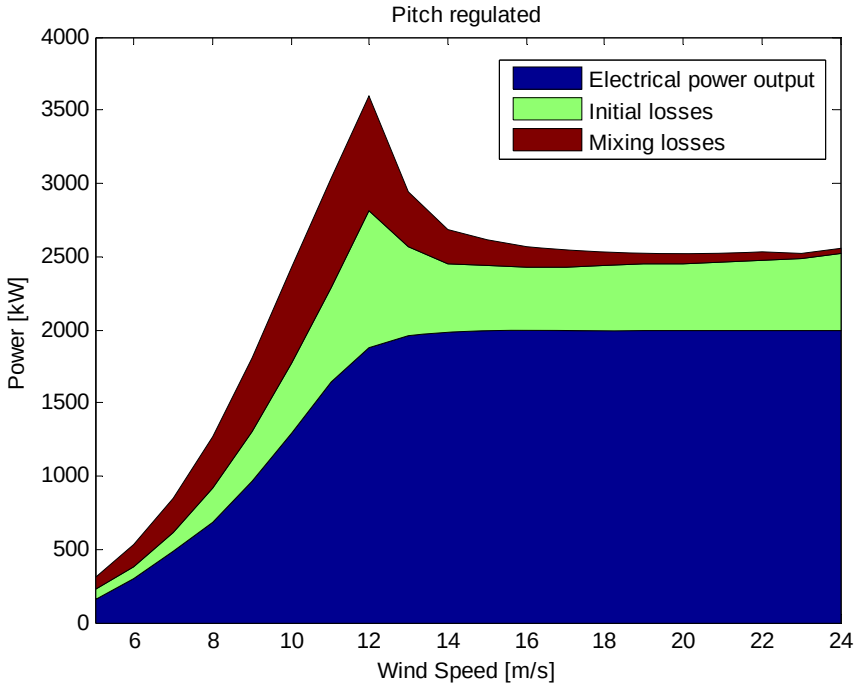

Figure 9: Comparison between the different powers computed using the thrust and power coefficients of a 2MW pitch regulated turbine (from manufacturer C_T and C_P curves).

A similar analysis can be done with an active stall regulated turbine as illustrated in Figure 10.

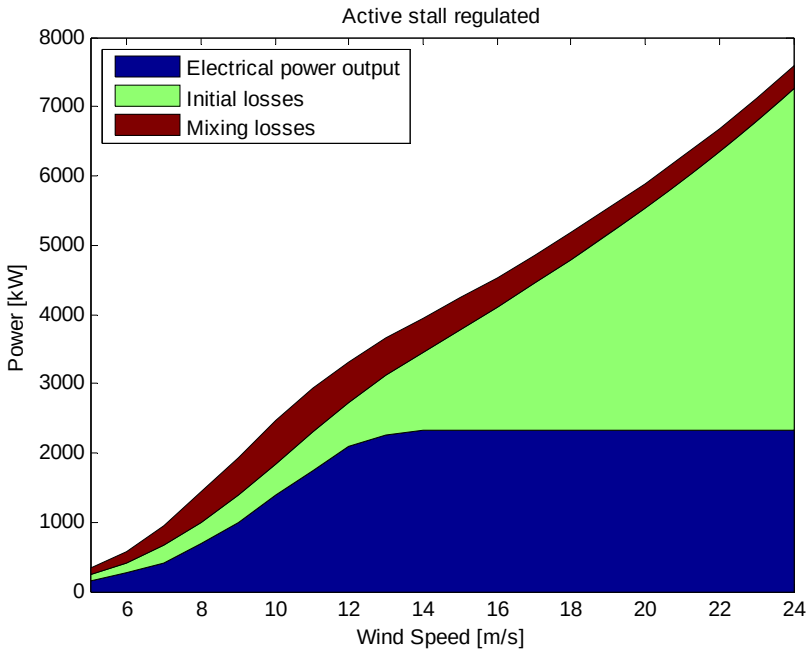

Figure 10: Comparison between the different powers computed using the thrust and power coefficients of a 2MW active stall regulated turbine (from manufacturer C_T and C_P curves).

The proportions are here different from the pitch-regulated turbine. The initial losses are increasing with respect to the wind speed. This observation can be explained by the fact that the wind turbine is pitching its blade to increase the stall effect on the blade in order to reduce the tangential loads and consequently the power. However, by doing this, the drag of the blades is slightly increased. Therefore, the thrust increases slightly after reaching the rated wind speed. As the kinetic power lost by the flow is the thrust multiplied by the wind speed, the kinetic power transferred to heat is expected to increase at a slightly faster rate than linearly.

From another point of view, the stall effect is concretely changing the position of the detachment of the flow on each section of the blades and therefore directly controlling the amount of turbulence generated by the blades. The sooner the flow is detached on the blade, the more turbulence is generated.

The mixing losses are staying almost constant after the rated wind speed, while they are reducing in the case of the Pitch regulated turbines. This can be explained by the thrust curve of the turbine, which has a very small increase after reaching the rated wind speed. If the C_T is constant, or slightly increasing, the relative deficit in wind speed in the wake will also slightly increase creating slightly more shear turbulence.

The same kinds of plots are presented in appendix C for each data set available. The proportions between the extracted power and the additional losses are a good visual check, to see if the methods to derive the thrust curves give physically realistic results.

3 Conclusion and future work

In order to propose robust guidelines design for wind turbine in cluster, the standards are intentionally made conservatives. By using the uncertainties of the thrust coefficient, and the power coefficient, the models describing the mean and turbulent flow field in wind turbine clusters could be designed, or calibrated more precisely. A long-term consequence would be a more optimized design of the wind turbines and the wind park layout, which would at the end reduce the initial and maintenance cost of the wind turbines, as well as increase the power production of the wind parks.

It is therefore of interest to develop standards describing precisely the methodology to estimate the thrust curve of a wind turbine and its corresponding uncertainty.

In the first two chapters, the equations of momentum and energy were developed in order to describe the interaction between the mean flow field, the forces applied on the wind turbine and the power extracted. The analysis remains nonetheless incomplete as a similar analysis on the turbulent field is missing.

Therefore, further work is needed on this subject to be able to “close” the system of equations: a derivation of the equations of motion in turbulent flow linking the wake width expansion with the dispersion and the dissipation of the shear turbulence (e.g. the so-called turbulence scale). And finally a physical relationship between the inflow turbulence, the thrust forces on the rotor and the wake width expansion. Without these set of equations, the wake of the turbine remains only partially known from empirical considerations.

Chapter III
Estimation of the thrust force and its combined uncertainty

In this chapter, three methods are proposed to determine the thrust and the thrust coefficient of wind turbines. The validity and the accuracy of the methods are then analyzed using real wind turbine data from various type and sources.

The first method presented uses wind speed measurements upstream and downstream a wind turbine to recreate the wake shape and to derive the thrust coefficient using the theory presented in Chapter I. The novelty of this method compared with the previous works found in the literature is to use a section of a cylinder control volume that takes into account the presence of the ground. The application of the method on real wind turbine measurement gives results in accordance with the thrust coefficient obtained from the wind turbine manufacturer. The uncertainty of the result is not determined rigorously, but the relatively high variations between one wind speed bin to another indicates a large sensitivity of the result accuracy to the quality of wind speed measurement.

The second method presented uses bending moments measured by strain gauges located on the wind turbine's tower. After the description of the different sources of bending moments on the tower, three methods are proposed and applied on four different instrumented turbines. The uncertainty of measurement of the methods is analyzed and applied on the data sets to quantify the combined uncertainty of the thrust curve. Different scenarios of input uncertainties are analyzed. The results agree with the manufacturer thrust curves in term of magnitude and shape. The combined uncertainty of the thrust curve is found to be very dependent of the strain gauge standard uncertainty as well as the wind speed standard uncertainty.

Finally, the third method proposed uses the Blade Element Method to derive the thrust curve. The novelty of the approach is, instead of using a model for the pitch and rotation speed control, the method uses real measurements inputs. The method is applied on an instrumented wind turbine using its airfoil data and different sensors to estimate the thrust for each 10-minute time series. The result, in comparison with the strain gauges measurements result, gives a similar shape with much less scatter. The uncertainty is estimated in a similar manner as with the strain gauge measurement method and is found to be of a significantly smaller order of magnitude.

1 Estimation of the thrust force from the wake shape

As it is presented in Chapter I, the wake wind speed distribution is directly related to the thrust coefficient of the turbine. It is therefore possible to estimate the thrust coefficient from a turbine by comparing the upstream and downstream wind speed. In order to validate the model developed, the thrust coefficient of wind turbines is derived using wake wind speed measurements in offshore wind farms.

1.1 Construction of the wake profile

In order to recreate the wind profile behind the turbine, the wind speed upstream a turbine is compared with the wind speed recorder downstream the turbine for different angles, as it is shown in Figure 11. The device used to record the wind speed downstream the turbine can be a met mast or another turbine (in that case, the wind speed is derived from the power output of the turbine, using an interpolation of the power output over the power curve, or a nacelle anemometer).

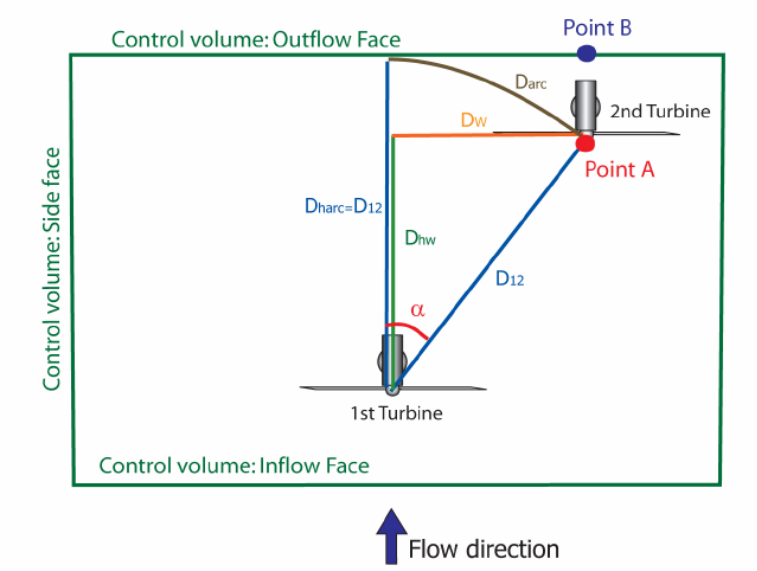

Figure 11: The wind speed seen by the 1st turbine is compared with the wind speed seen by the second turbine for different wind direction angles.

The result is a wind speed ratio as a function of a wind direction (Figure 12).

Using a simple trigonometry transformation (III-1.1), the wind direction can be transformed into a radial distance from the wake centerline. With the distance between the two turbines D_{12}, and the angle between the wind direction and the row of turbine α.

$$\boxed{D_W = D_{12}\sin(\alpha)} \qquad \text{(III-1.1)}$$

The problem with this method is that the wind speeds recorded are not exactly at the same axial distance from the turbine (on Figure 11, the point A and B are assumed to have the same wind

speed). There is an axial error which increases with the direction angle: $Error = D_{12}\left(1-\cos\left(\alpha\right)\right)$. Therefore, this method is only acceptable for a small angle alpha.

1.2 Wake width definition

Another problem with these methods is the definition of the wake width by itself. As the wake width determines completely the result of the analytical method and partly the one of the numerical method, the precision in its derivation is crucial. The first idea would be to define the wake width as the distance between the centerline and the first point where the wind speed ratio is equal to unity. However, the position of this point is highly dependant on the smoothing method used, and is not relevant to the definition of the bell shape, which tends to unity at infinity.

What can be measured with a relative accuracy is the factor k/R^2, in the definition of the bell shape (III-1.2). This factor quantifies the width of the bell shape in a normalized coordinate. If R is defined as the wake width radius, k is then a non-dimensional factor, which determines the area radius over which the integration is carried on. In other words, k determines the amount of the shape that will be taken into account. The decision of the value of k will therefore have an influence on the final result. This dependency of the integration with regards to k is coming from the definition of the wake shape as a function that does not have a radial limit (the deficit is converges to zero at infinity). In order to define the wake width, the function needs to have a radial limit, which has to be defined empirically.

Ideally, k should be taken as big as possible in order to encompass the maximum effect of the wake inside the control volume. However, in practice, it can be used as an empirical parameter to *calibrate* the model to measurements.

$$U_w\left(r\right) = U_\infty - \left(U_\infty - U_{\min}\right)e^{-k\left(\frac{r}{R_w}\right)^2} \qquad \text{(III-1.2)}$$

In order to integrate the wake shape analytically, the wake width must be determined from the wake shape properties. In order to do that, a normal distribution is fitted over the wake shape.

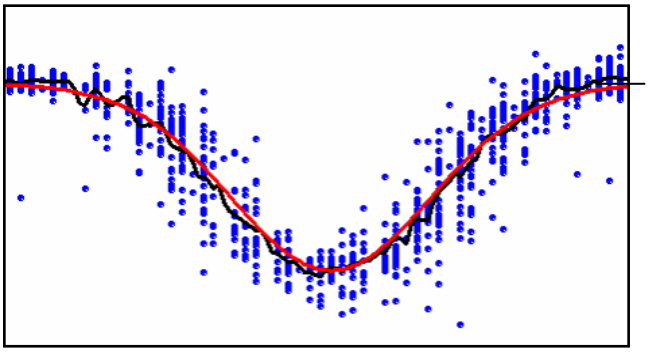

Figure 12: Wake shape ($U_w(x)/U_{inf}$) with respect to the distance from the centerline (the blue points are 10-minute averages, and the black line is the mean value) on which a normal distribution is fitted (red line).

1.3 Self similarity verification

One of the most critical assumptions of the methods presented is concerning the self-similarity of the normal distribution of the wake. In order to validate this assumption, the wake shape from different wind turbines are plotted over a distance scaled over the wake shape at various wind speed.

Horns Rev, p. 109: Figure 89, and Figure 91

Middelgrunden, p.118: Figure 106, Figure 108

The results found corroborate that the assumption of self-similarity, with a normal distribution, seems to be acceptable after six rotor diameters. Before six rotor diameters, the example of Middelgrunden shows that the head of the shape seems to be steeper than a normal distribution, closer to a "top hat" distribution. This is maybe because the shear forces turbulence have not reached the wake centerline yet, so the shape of the induced velocities is still visible. Nonetheless, the wake shape measured at Middelgrunden is expected to have a significant error coming from the method used to obtain it. As it is explained previously, the method is assuming that the wind speed measured at one point behind the turbine with different inflow angle is the same as the wind speed projected orthogonally on the outflow surface of the control volume. The measurement is done at 2.3 rotor diameters downstream the turbine. The error will therefore be, here, quite large and will tend to under predict the wind speed deficit more and more at an increasing radial distance from the centerline. The effect on the wake shape should give steeper slopes. With a model of the wake width expansion and centerline wind speed expansion valid at a short distance from the turbine, this effect could be corrected through an iterative method.

After 6 rotor diameters, the wake shape can be fitted by a normal distribution for their central parts, on the "edges", the Gaussian distribution generally slightly underestimate the deficit. This error seems to be independent of the wind speed or the distance as there are no visible trends. This difference could partly be explained by the same error acting on Middelgrunden's wake shape but on a smaller amplitude.

1.4 Numerical method

Both the numerical method and the analytical method are based on solving the equation (III-1.3).

$$\boxed{C_T = 2\frac{A_w}{A_T}\left(\overline{f} - \delta_{\min}\overline{f^2}\right)\delta_{\min}} \qquad \text{(III-1.3)}$$

The numerical method is based on a numerical integration of the wake shape without assumption made over the distribution of the wind speed in the wake except the axial symmetry. Neither the wake width nor an analytical formulation of the wind speed distribution is needed. The idea is to take one-half of the wake shape and to assume that this wind speed deficit is the same around the axis of the centerline. The wake shape can then be integrated over the disc section, defined in Chapter II, by splitting the integral on the two parts of the disc: the slice and the triangle (III-1.4), with the area of the disc section defined as $A_0 = H\sqrt{R^2 - H^2} + R^2\left(\pi - \beta\right)$. As the disc section is not axis symmetric, the square of the spatial averaged wake shape is not the same as the spatial averaged

of the squared wake shape $\overline{f^2} \neq \overline{f}^2$. The spatial averaged of the squared wake shape need also to be integrated numerically in the same way (III-1.5).

$$\boxed{\overline{f} = \frac{1}{A_W}\left(2\tan(\beta)\int_0^H \Phi(r)\,r\,dr + 2(\pi-\beta)\int_0^R \Phi(r)\,r\,dr\right)} \quad \text{(III-1.4)}$$

$$\overline{f^2} = \frac{1}{A_W}\left(2\tan(\beta)\int_0^H \Phi^2(r)\,r\,dr + 2(\pi-\beta)\int_0^R \Phi^2(r)\,r\,dr\right) \quad \text{(III-1.5)}$$

This method, which requires fewer assumptions than the analytical method, gives a different result for each side of the wake deficit (left and right) and is slightly dependent on the smoothing algorithm, the numerical integration method function, and the integration length *R* used.

1.5 Analytical method

The analytical method, also based on equation (III-1.3), assumes a normal distribution on top of the assumption of self similarity and axis symmetry. The first step is therefore to fit a bell shape over the wake deficit, which gives the wake width defined in section Chapter I1.7.3 From this step the spatial integration of the wake shape can be derived from equation (III-1.6), presented in section Chapter I1.7.3 with $\eta = H/R$, and $\beta = \arccos(\eta)$.

$$\boxed{\overline{f_k} = \frac{\left(1-e^{-k\eta^2}\right)\sqrt{1-\eta^2} + \eta\left(1-e^{-k}\right)(\pi-\beta)}{k\eta^2\sqrt{1-\eta^2} + k\eta(\pi-\beta)}} \quad \text{(III-1.6)}$$

The integration of the square of the wake shape is found by solving equation (III-1.6) using a 2*k*. As the function has the following property: $\overline{f_k^2} = \overline{f_{2k}}$.

1.6 Results

The two methods are compared with real wind turbine data from the Danish offshore wind farms Horns Rev and Middelgrunden. In each wind farm two turbines are selected and the wind speed measured at the first one is compared with the wind speed measured at the second one. Both the wind speed measured at the nacelle anemometer and derived from the power output are available. Because of the limitation of the wind speed from the power output (the way of deriving the wind speed is interpolating the wind speed over the power curve, and do not work for wind speed higher than the rated wind speed), the wind speed measured at the nacelle anemometer is preferred in order to obtain the thrust coefficient for as many wind speed bins as possible. The plots are presented in Appendix C:

Horns Rev, p.111: Figure 92, Figure 94, Figure 96, and Figure 99.

Middelgrunden, p.120: Figure 109, Figure 111, and Figure 113.

For Horns Rev, both the analytical method and the numerical method give similar results if the integration width used is the same as the wake width found from the bell shape fitting method. The C_T results for the two methods are then dependant on the accuracy of the bell shape fitting with the wake shape, and the more the shape is similar to the bell shape, the more the results are found to be in accordance.

In the case of Middelgrunden the assumption of self similarity is not respected as the wind turbines are spaced at 2.3 rotor diameters and the wake structure did not expend totally before reaching the next turbine. The consequence on the result is that the analytical method is clearly off in comparison with the two numerical method results.

In both cases, for a constant $k=2$, the results are in good agreement in term of shape and order of magnitude in comparison with the manufacturer C_T curve.

There is a relatively large variation of the C_T from one wind speed bin to another. This fact shows how sensitive the methods are to the accuracy of the data. Despite an effort to improve the robustness of the methods by using robust smoothing functions resistant to outliners, the uncertainty of the wind speed and wind direction seems to influence greatly the uncertainty of the final C_T result. Nonetheless, while in Horns Rev cases the measurements downstream the turbine are done at more than 7 rotor diameters, which generates a relatively large amount of noise in the wake shape and could explain the large variations on the C_T curve, Middelgrunden's measurements are done at only 2.3 with a better yaw sensor and give even larger variations. So the large variations cannot only be attributed to the measurements inaccuracy.

The factor k has a significant influence on the results. It tends to give an increase in the thrust coefficient for an increase in the k value. This can have several interpretations:

- The wake shape is not symmetric vertically, and this assumption over predict the amount of wind deficit under and/or higher the hub height.
- The wind direction sensors are not precise enough to give a realistic wake shape and tend to over predict the wake width.
- There are unsteady phenomena, which have a significant influence over the averaged wind speed or wind direction values. For instance, the so-called wake meandering, which has a relatively high frequency compared to 10-minute mean time series [Medeci, 2006, p.167], may have an effect on the wake width measurement.

Nonetheless, using the factor k=2 give fine results for the C_T in term of order of magnitude and shape for both cases.

1.7 Uncertainty

1.7.1 Main factors of uncertainty

a) Wind direction sensor

One of the main sources of uncertainty is the wind direction sensor. Indeed, its accuracy reflects the accuracy of the wake shape. Therefore, a high random error on the wind direction can have the effect to blur the shape of curve by widening the wake width and decreasing the centerline deficit.

The wind direction sensor can whether be a wind vane on a met mast or the yaw direction sensor of the turbine.

Wind vanes are in general relatively accurate with a resolution between +/- 2° and +/- 5° [Windspeed.co.uk]. Yaw sensors have probably an accuracy of a similar order of magnitude.

Another issue is due to the geographical coherence between the met mast and the turbine considered. After several kilometres, even in offshore context, the wind direction can easily be randomly changed by several degrees. Furthermore, the wind direction measured by met mast in the shadow of turbines is significantly affected by the wake turbulence, which makes them inappropriate as a source of wind direction.

b) Wind speed sensor

The wind speed sensor contributes also a lot to the final uncertainty of the C_T curve. In the two cases studied the wind speed sensors available for this task are the nacelle anemometers and the power production of the turbine. Both have a very poor precision and have an uncertainty of at least +/-0.5 m/s.

c) Amount of data

The amount of data plays a significant role in reducing the uncertainties of the wake shape. As it is presented in the Appendix B, the type A standard uncertainty is related to the standard deviation of the data divided by the square root of the amount of data available. The more data available, the more the type A uncertainty are reduced. Nonetheless, the amount of data has no influence on type B uncertainties, as they partly encompass biased errors.

d) Smoothing algorithm

The smoothing algorithm used also plays a significant role in the final wake shape. The program uses different methods. The most basic one is based on fixed bins in which the averaged values are computed. While this is the method recommended in the standards for deriving power curves, it is not ideal to obtain a smooth curve, as each point of the curve is independent of the others. The other methods are therefore based on a sliding bin method, where part of the points used to average a bin, are also used in the neighbouring bins.

An advanced method is used, using a *locally weighted scatter method*. Instead of according an equal importance of the point located inside the bin, their importance is *weighted* in accordance to their distance from the center of the bin. The weights used can be derived from a linear polynomial, or a

quadratic polynomial least square regression. In order to make the smoothing process more robust, the outliners are excluded from the smoothing by computing the residual of the mean with the scatter points, and by excluding the ones that are too far from the deviation of the residuals (typically a factor of 6 is used) [Matlab Help, Curve fitting toolbox].

Using the most basic method gives rather poor results, which are improper to fit the wake shape by a normal distribution. The moving average is giving better results, especially using the locally weighted scatter method with a pre-processing to exclude the outliners. The span used has a very big influence on the final shape, with a tendency to flatten the curve for high values. It is therefore defined visually by making a fair compromise between the smoothing of the shape and preserving the information describing the wake properties (maximum deficit, and wake width).

1.7.2 Uncertainty estimation of the wake shape thrust coefficient

Estimating the combined uncertainty of the resulting thrust coefficient is very complicated, as it has to take into account every step, from the creation of the wake shape to its integration. While in theory it should be possible, in practice the propagation of the uncertainty generated by the smoothing method, and the bell fit over the wake width represents a special situation that is not found to be documented. A serious mathematical study is here necessary to propose a robust method to estimate the propagation of this uncertainty. Further work is therefore needed on this part to estimate the combined standard uncertainty of the thrust coefficient derived from the wake shape.

1.8 Conclusion

The methods proposed are giving results in agreement with the manufacturer C_T curves which validate the physical relationship between the thrust and the wind speed deficit presented in Chapter I. Nonetheless, the sensitivity of the methods regarding the accuracy of the measurement is found to be far too great to give a precise description of the thrust coefficient.

Nonetheless, the methods can be significantly improved with, for instance, a more robust method to smooth the curve and to determine the wake width. In addition, with further assumptions on the inflow and outflow profile a more realistic method could be designed to solve the momentum equation and to estimate the thrust coefficient. Furthermore, a model estimating with precision the uncertainty of the results is needed. Finally, the new method should be compared with more accurate data in term of wind speed and wind direction. An isolated wind turbine with several met masts located at various distance could be used to determine with a greater precision the wake shape.

2 Estimation of the thrust from tower bending moments measurements

The axial wind forces applied on the rotor of the turbine creates bending moments on the tower and the foundations. Using strain gauges, the bending moments can be recorded at any position on the tower. Therefore, it should be possible to measure the bending moments generated by the thrust on the tower, and ultimately to derive the thrust itself from these measurements. The problem is that the thrust is only one component of various moments created by the complex interaction between the wind flow field, the gravity field and the turbine. A model taking into account the major moments applied on the tower is therefore needed to be able to derive the thrust from strain gauges measurements. This model can be used to quantify the influence of the uncertainty of each parameter taken into account on the combined standard uncertainty of the thrust using the method presented in Appendix B.

Unfortunately, there was not any literature found dealing with the subject of modelling the tower bending moments generated by the thrust. The models proposed in this section are therefore derived from general knowledge about the bending moments and the forces applied on a turbine, and the suggestions of referenced professionals from Risø, Siemens, and Elsam Engineering.

The models are used to estimate the thrust with strain gauges measurements from the different data sets. While they give rather good results with strain gauges located at the bottom of the tower, the resulting thrust curve becomes less and less convincing for strain gauges located at an increasing height on the tower, which underlines the limits of the assumptions taken.

2.1 Strain gauge description

Strain gauges are devices used to measure the deformation of objects. The most common type of strain gauge consists of a flexible backing, which supports a metallic foil pattern. As the object is deformed, the foil pattern is deformed, causing its electrical resistance to change. This resistance change can be used to calculate the exact amount of deformation. In order to monitor the resistance change, a Wheatstone bridge can be used. This device measures the exact value of the resistances, through measuring the voltage between the two midpoints (Figure 13)

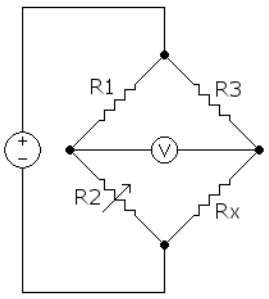

Figure 13: A simple Wheatstone bridge for measuring Rx, with R1, R2 and R3 known

According to the precision needed, several strain gauges set up can be used with the Wheatstone bridge.

A simple bridge (or quarter bridge) uses only one strain gauge and three equally balanced resistances. It can be influenced by temperature (the strain gauge are more affected than the resistance by temperature, which creates an unbalance). It has also a small output, so might generate too much noise in some occasions [Iotech].

A half bridge is using two strain gauges, which gives a stronger signal than the quarter bridge (with less noise), but is still influenced by temperature.

Finally, a full bridge is a setup of four strain gauges (one for each resistance) mounted on the test surface (two on each opposite side of the surface). This setup cancels the effect of temperature, as all the strain gauges will be influenced equally.

While the full bridge is in general considered to give the most accurate results, and is less sensitive to local effects than the half bridge or even the quarter bridge, it is practically more complex to set up. Indeed, it has to be located on both side of the surface. The half bridge is therefore more generally used for tower bending moments [Balling, 2006, p.11]. The consequence is that, in the data sets, the strain gauges measurements are partially dependent of ambient temperature.

2.2 Location on the turbine

The strain gauges measuring the thrust are located on the bottom part of the turbine. They are usually placed in couple at the same height with a relative angle of 90° between one another. Practically it can be difficult to position the strain gauges exactly at 90°, and therefore the model presented in the following sections is considering a random angle between the two strain gauges (α_1 and α_2 on Figure 14).

The coordinate system used with the bending moments is fixed on the nacelle, and is therefore dependent of the wind direction (Figure 14). The Z-Axis is positioned in the same direction as the wind direction while the Y-Axis is vertical and oriented toward the sky, and the X-Axis is completing the Cartesian coordinate (X,Y,Z).

In order to be able to compare the bending moments a sign convention has to be set up. The bending moments are considered positives if they are bending the tower in the direction of the Cartesian coordinate and negative otherwise. In this convention, the thrust bending moment, which bends the tower in the Z-direction, is positive.

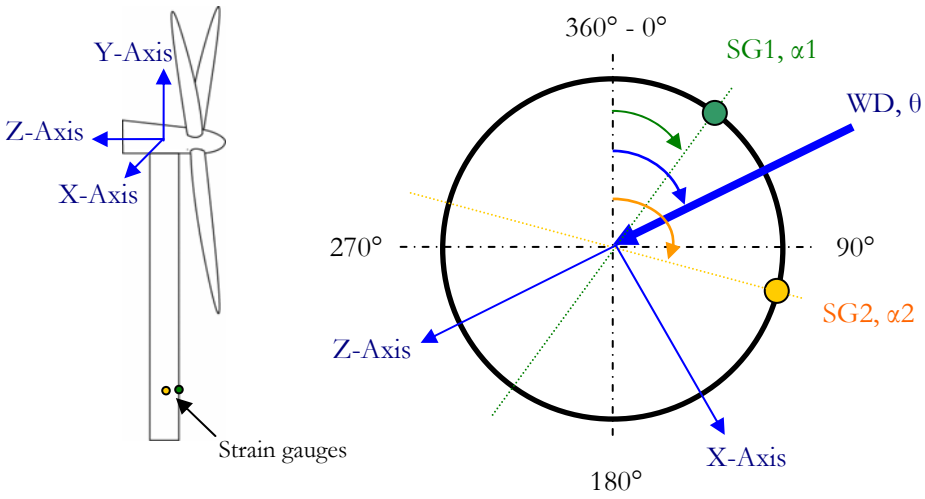

Figure 14: Location of the strain gauges on the tower

2.3 Calibration procedure of the tower bottom strain gauges

The calibration of strain gauges are done by applying a load through a load cell on a pull point on the turbine (e.g. at the hub of the nacelle) and by relating the load cell measurement with the strain gauge measurement

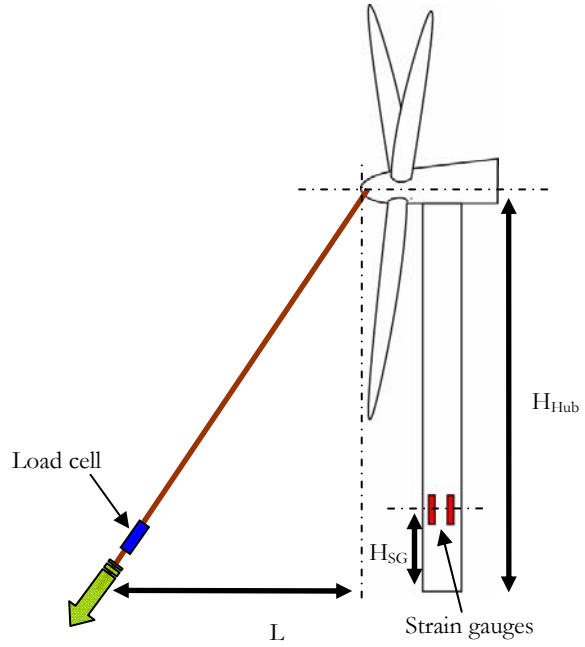

Figure 15: Calibration procedure [Balling, 2006, p.32]

The first step is to calibrate the load cell properly, in order to obtain the corresponding load from the voltage measurement. This can be done using the calibration certificate given with the load cell. The next step is, then, to pull a cable attached on the tower/nacelle at a known distance from the

strain gauge (Figure 15). The load cell fixed on the cable measures the load applied on the tower top. This load can be transformed into a bending moment using equation [Balling, 2006, p.38].

$$BM_{SG} = \left(H_{Hub} - H_{SG}\right) \cdot F \cdot \cos\left[\arctan\left(H_{Hub} / L\right)\right] \tag{III-2.1}$$

The calibration, using this method, does not take into account the gravity moment generated by the mass of the rotor. In order to correct the strain gauge measurement to considering the gravity moment, the nacelle is turned of 360° while recording the strain gauge measurement [Jensen, 2006; Balling, 206]. Plotted against the wind direction the signal gives a cosines curve, which has to be centred to zero to account for the gravity.

2.4 Strain gauge model

In order to derive the thrust coefficient from the strain gauge signal, a proper model of the relationship between the strain gauge measurement and the turbine behaviour has first to be set up. For this purpose, the various forces acting on the turbine and their influence on the strain gauge have to be considered.

2.4.1 Relationship between bending moments and strain gauge measurements

As it is described previously, two strain gauges are placed on the tower. They are positioned in general at 90° from one another. However, it can be interesting to assume this angle to be random, in order to be able to correct a possible error of placement. As their position is fixed on the tower, they are not aligned with the coordinate system of the nacelle presented previously (Figure 14). The forces expressed in this system have therefore to be projected on the strain gauge coordinate system in order to model the bending moment measured by the strain gauge.

The formula modelling the strain gauge measurement is therefore (III-2.2), with the strain gauge i measurement defined as SG (with the correct gain and offset), the bending moment in the z-direction BM_z, the bending moment in the x-direction BM_x, the wind direction θ_{wind}, and the relative angle of the strain gauge position toward the north in a clockwise angular coordinate α [Jensen, 2006].

$$SG_i = BM_z \cos\left(\theta_{wind} - \alpha_i\right) + BM_x \sin\left(\theta_{wind} - \alpha_i\right) \tag{III-2.2}$$

If there are two strain gauges available, a relationship between the bending moments and the strain gauge is easily derived to equation (III-2.3) using the trigonometry relationship (III-2.4).

$$\begin{cases} BM_z = \dfrac{SG_1 \sin\left(\theta_{wind} - \alpha_2\right) - SG_2 \sin\left(\theta_{wind} - \alpha_1\right)}{\sin\left(\alpha_1 - \alpha_2\right)} \\ BM_x = \dfrac{SG_2 \cos\left(\theta_{wind} - \alpha_1\right) - SG_1 \cos\left(\theta_{wind} - \alpha_2\right)}{\sin\left(\alpha_1 - \alpha_2\right)} \end{cases} \tag{III-2.3}$$

$$\sin(\alpha_1-\alpha_2)=\cos(\theta-\alpha_1)\sin(\theta-\alpha_2)-\cos(\theta-\alpha_2)\sin(\theta-\alpha_1) \quad \text{(III-2.4)}$$

An alternative method is to derive the norm of the bending moment from equations (III-2.3), in order to drop the dependency to the wind direction. This norm is referenced later on as the total bending moment.

$$\boxed{\|BM\|^2 = BM_z{}^2 + BM_x{}^2 = \frac{SG_1{}^2 + SG_2{}^2 - 2SG_1SG_2\cos(\alpha_1-\alpha_2)}{\sin(\alpha_1-\alpha_2)^2}} \quad \text{(III-2.5)}$$

This solution is completely independent of the wind direction and is a good check to verify if the strain gauge angle is accurate, and to check if the gain and offset of the strain gauges are balanced between one another.

2.4.2 The different forces measured by the tower bending moment

The strain gauges on the tower base of the turbine measure various interactions between the system and the turbine. Indeed, as the strain gauges are located at the bottom of the tower, most of the forces acting on the wind turbine contribute to the bending moment measured.

o The rotor mass bending moment

The mass of the wind turbine contributes to the bending of the tower by applying a moment at its top. This moment is roughly equal to the mass of the rotor multiplied by the shaft length (more precisely to the distance between the rotor position, and the center of the tower), and by the gravity constant g (III-2.6). In practice, it is very difficult to estimate with precision the bending moment generated by the rotor mass. Nonetheless, it is possible to measure it during the calibration of the strain gauges by rotating the nacelle of 360° and plotting with respect to the nacelle direction.

The rotor weight is acting only in the Z-direction. According to the sign convention presented before, the moment has a negative value. The moment is the same at any height on the tower as it can be considered to be a pure moment acting the tower top [Paulsen, 2006].

$$\overrightarrow{BM_{Rotor}} = -M_{rotor}\cdot L_{shaft}\cdot g\cdot \vec{e_z} \quad \text{(III-2.6)}$$

It can be argued that the rotor mass also contributes to create a moment on the tower top over the Z-axis with a sign and amplitude depending of the azimuthal position of the blade. However, as the time series considered are 10-minute averages, with the symmetry of the rotation, the contribution is assumed to be null in average.

o The thrust bending moment

The thrust force is applied on the tower top in the Z-direction (if the nacelle is aligned with the wind direction). The corresponding bending moment applied on the tower is therefore equal to the force multiplied by the distance between the tower top (H_{Hub}) and the location of the strain gauge measuring it (H_{SG}). The force is applied on the rotor in the Z-direction, therefore the sign of the bending moment is positive (III-2.7) [Paulsen, 2006].

$$\overrightarrow{BM_{Thrust}} = Thrust\cdot x\cdot \vec{e_z} = Thrust\cdot(H_{Hub}-H_{SG})\cdot \vec{e_z} \quad \text{(III-2.7)}$$

o The tower drag bending moment

The wind is also acting on the tower and is creating a corresponding bending moment at the tower bottom. As the force is distributed over the section area of the tower, it is integrated to derive the bending moment. The formula is therefore the integral of the force acting on an infinitesimal area of the tower multiplied by the distance from the strain gauge (III-2.8). As the tower radius decreases significantly over the tower height (from R_0 to R_{Hub}), this is taken into account by assuming a linear decrease of the tower radius [Paulsen, 2006].

$$\overrightarrow{BM_{Tower}} = \int_{H_{SG}}^{H_{Hub}} \frac{1}{2} \rho C_D U^2 \cdot \pi \left(\frac{r}{H_{Hub}} \left(R_{Hub} - R_0 \right) + R_0 \right) \cdot \left(H_{Hub} - r \right) \cdot dr \cdot \vec{e_z} \qquad \text{(III-2.8)}$$

The tower drag bending moment after integration is

$$\boxed{\overrightarrow{BM_{Tower}} = \frac{1}{12 H_{Hub}} \cdot \pi \rho C_D U^2 \left(H_{Hub} - H_{SG} \right)^2 \left(H_{Hub} \left(2R_{Hub} + R_0 \right) + H_{SG} \left(R_{Hub} - R_0 \right) \right) \cdot \vec{e_z}} \qquad \text{(III-2.9)}$$

The tower drag could be even more precise by considering the inflow profile: instead of using only the wind speed at hub height, the wind speed would be taken as a logarithmic profile and integrated over the height of the tower. For doing this, the roughness of the terrain around the turbine should be measured properly and applied to the logarithmic profile according to the wind direction. The difference between this method and (III-2.9) is nonetheless expected to have a very small impact on the final bending moment and the simplified model is therefore kept.

o The torque

The torque of the rotor acting on the generator shaft is also contributing to the tower bending moment. However, as the rotation of the rotor is done over the Z-axis (i.e. in the X-direction), the bending moment is felt by the tower in the X-direction with a sign depending of the direction of rotation of the rotor. The bending moment can be derived from the power output and the rotor rotation speed or directly from the shaft torsion measured through a strain gauge [Jensen, 2006].

$$\overrightarrow{BM_{Torque}} = \pm \frac{Power}{RotationSpeed} \cdot \vec{e_x} = \pm Torsion_{Shaft} \cdot \vec{e_x} \qquad \text{(III-2.10)}$$

In the case of Siemens, the two methods to derive the torque are found to be in close agreement.

o Tilt moment

Finally, the tilt moment of the turbine can also influence the bending moment measured on the tower. In fact, the difference of wind speed between the upper part and the lower part of the rotor can create a moment applied on the shaft at the connection with the rotor. This moment is propagated to the bottom of the tower where it is added up to the other contributions. In general, this tilt moment depends of the inflow wind profile, which changes according to the wind speed and the roughness of terrain seen by the incoming flow. However, other parameters can influence it greatly, like the temperature of the air and the ground, which influence its profile.

This moment can be directly calculated from the instantaneous rotating shaft bending moment transposed on the fixed wind turbine coordinate system. The moment is applied in the Z-direction

with a sign depending of the wind profile (in general, the sign will be positive as the wind profile normally follows an increasing trend at hub height).

$$\overrightarrow{BM_{Tilt}} = BM_{Shaft} \cdot \vec{e_z} \tag{III-2.11}$$

Unfortunately, the tilt is not available in most of the data sets. The only case where the tilt is available (Siemens), the tilt has a shifting that cannot be corrected. It is therefore assumed in all the computation that the tilt is null.

o Combined bending moments

So the different moments that contribute to the tower bottom bending moment seen by the strain gauges can be gathered into the bending moment in the z-direction, which include the thrust bending moment, the rotor weight moment, the tower drag bending moment and the tilt moment. And the bending moment in the x-direction is done by the torque [Jensen, 2006].

$$\begin{cases} BM_x = BM_{Torque} \\ BM_z = BM_{Tilt} + BM_{Rotor} + BM_{Thrust} + BM_{Tower} \end{cases} \tag{III-2.12}$$

2.4.3 Influence of the different forces

In order to study the influence of the different forces on the resulting bending moment measured on the tower, each bending moment is plotted on Figure 16 with respect to the wind speed at two different heights (55m from the hub and 4m from the hub, on a 60m high tower). As it can be seen, the influence of the rotor mass and the rotor torque are largely dominant at 4m and drive totally the shape of the resulting total bending moment (the norm of BMz and BMx). At lower location on the tower, the main contribution to the total bending moment is coming from the thrust, and in part from the tower drag force at high wind speed. The rotor weight and the torque play a more limited influence.

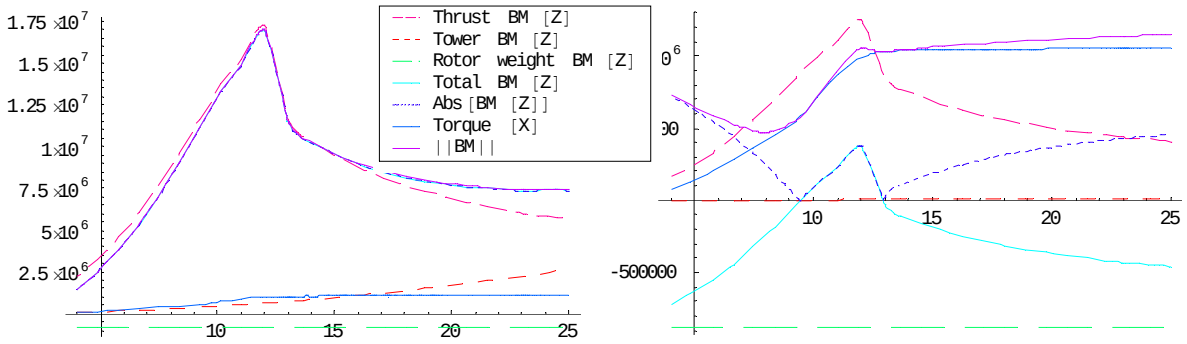

Figure 16: Simulation of strain gauge bending moments applied on the tower [Nm], at 55m from the hub (left) and 4m from the hub (right) versus wind speed [m/s]. The colors indicate the different moments considered.

This difference of origin of contribution has a direct repercussion on the strain gauge measurements. For instance, at low height on the tower, the strain gauge will measure a bending moment essentially in the z-direction, and therefore will see a cosine-like oscillation of the bending moment with respect to the wind direction, because of equation (III-2.2). On the other hand, for an

increasing height, the influence of the torque (so the x-direction bending moment) will be more and more important in comparison with Z-direction bending moments. This is particularly visible on Figure 17 at 4m (right), where the oscillations with respect to the wind direction go from a cosine-like curve at low wind speed because they are driven by the z-direction bending moments to a sinus-like curve at high wind speed as the influence of the torque (x-direction bending moment) is increasing. This effect is also visible on real the strain gauges measurements, in the case of Horns Rev, and can be seen in the Appendix C1 (see Figure 33, p.75).

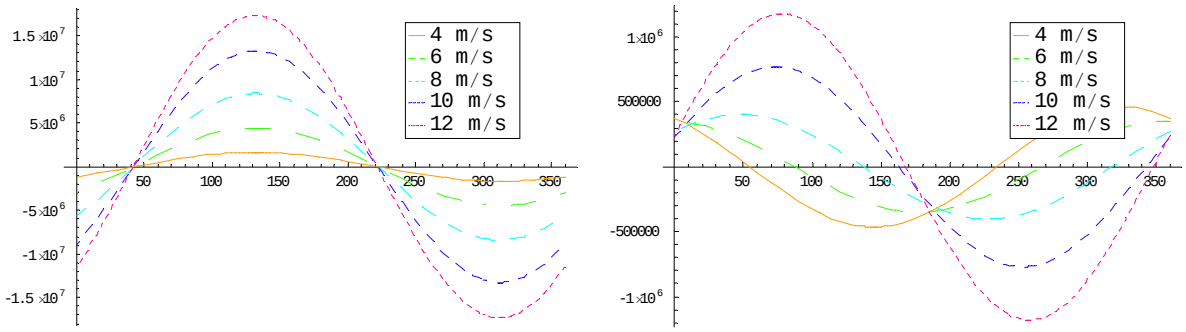

Figure 17: Simulation of a strain gauge bending moments [Nm] versus wind direction [°], at 51m from the hub (left) and at 4m from the hub (right) with the same radial position on the tower. The colors indicate the wind speed bins [m/s]

The influences of the different forces even if some of them are found to be very small at lower wind speed need to be taken into account in the derivation of the thrust coefficient from the strain gauge measurement.

2.4.4 Derivation of the thrust

o Using one strain gauge [Method 1]

The derivation of the thrust can be done with different methods. The simplest method is to use only one strain gauge, and to project it on the Z-axis of the nacelle. In order to do that, the wind directions that are too close to the perpendicular angle of the strain gauge position angle have to be excluded in order to avoid division by zero errors.

$$Thrust_1 = \frac{1}{H_{Hub} - H_{SG}} \left(\frac{SG_i - BM_{Torque} \sin\left(\theta_{wind} - \alpha_i\right)}{\cos\left(\theta_{wind} - \alpha_i\right)} - BM_{Rotor} - BM_{Tilt} - BM_{Tower} \right) \quad \text{(III-2.13)}$$

o Using two strain gauges without the torque [Method 2]

The second method that can be used is to use both strain gauges in order to eliminate the expression of the torque.

$$Thrust_2 = \frac{1}{H_{Hub} - H_{SG}} \left(\frac{SG_1 \sin(\theta_{wind} - \alpha_2) - SG_2 \sin(\theta_{wind} - \alpha_1)}{\sin(\alpha_1 - \alpha_2)} - BM_{Rotor} - BM_{Tilt} - BM_{Tower} \right) \quad \text{(III-2.14)}$$

o Using two strain gauges without the wind direction [Method 3]

Finally when the wind direction sensor has a high standard uncertainty, the two strain gauges can be used to derive the norm of the bending moment seen in equation (III-2.5).

$$Thrust_3 = \frac{1}{H_{Hub} - H_{SG}} \left(\pm \left| BM_z \right| - BM_{Rotor} - BM_{Tilt} - BM_{Tower} \right) \quad \text{(III-2.15)}$$

With $BM_{\tilde{z}}$ derived from equation (III-2.5):

$$BM_z^2 = \frac{SG_1^{\,2} + SG_2^{\,2} - 2SG_1SG_2 \cos(\alpha_1 - \alpha_2)}{\sin(\alpha_1 - \alpha_2)^2} - BM_{Torque}^2 \quad \text{(III-2.16)}$$

This method has a major drawback: the sign of $BM_{\tilde{z}}$ cannot be found directly from the set of equations. As it can be seen in the previous section, the bending moment in the z-direction is largely influenced by the rotor weight at low wind speed, and there might be a negative bending moment when the thrust and tower contribution are lower than the rotor weight moment. If this is the case, this sign needs to be corrected. A possible method could be to obtain the sign from the first method and using the strain gauge that has the smaller relative angle with the wind direction (to avoid the division by zero issue).

$$Sign(BM_z) = Sign\left(\frac{SG_i - BM_{Torque} \sin(\theta_{wind} - \alpha_i)}{\cos(\theta_{wind} - \alpha_i)} \right) \quad \text{(III-2.17)}$$

Practically this solution fails sometimes by giving negative values of the thrust, and eventually generates outliners that have to be excluded from the curve smoothing. This is mainly due to wrong wind direction values, or too weak strain gauge signal.

o Deriving the thrust coefficient

The thrust coefficient can then easily be derived from one of the three expressions of the thrust presented, by dividing it by one-half of the rotor area multiplied by the air density and the wind speed squared.

$$C_T = \frac{Thrust}{½ \rho \pi R_T^{\,2} U^2} \quad \text{(III-2.18)}$$

2.4.5 Global results

o Procedure followed to derive the global results

The thrust is derived for the different data sets presented in Appendix B, i.e. for Horns Rev's Vestas V80/2000, Tjæreborg's Neg Micon NM80/2750, Høvsøre's Siemens S93/2300 and Risø's Nordtank N35/550. The three first turbines are variable speed active pitch regulated wind turbines,

while the Nortank turbine is single speed and stall regulated. There is a large difference of scale between the three pitch turbines, which have a rotor diameter of more than 80m, and the stall turbine, which has a rotor diameter of 35m. A comparison based on the power control mechanism is therefore not as straight forward as it could have been if some measurement data of a large stall or active stall wind turbine would be available.

The first step of the procedure followed to analyze each set of data, is to filter the data of the abnormal cases, where the wind turbine is acting in an unexpected manner. To carry on this task, different sensors are plotted against other correlated sensors to identify the outliners visually, and automatically, through a robust curve fitting function. Generally, the power curve, pitch curve and generator rotation speed curve plotted with respect to the wind speed give a good proportion of the outliners. Other sensors can be filtered using boundaries, determined from general knowledge of the normal conditions. E.g., the wind direction sensor can be used to exclude area where the wind speed is known to have a high inflow turbulence because of the presence of other wind turbines or large bodies creating wake turbulences; the yaw error sensor is also a good indicator to exclude abnormal conditions. The different filter cases used are illustrated in the following figures:

- Horns Rev, p.72: Figure 26, and Figure 27.
- Siemens, p.132: Figure 132, Figure 133, Figure 134, and Figure 135.
- Neg Micon: . The data is already filtered and do not require to exclude any further data to obtain a satisfying thrust curve.
- Nordtank, p.172: Figure 198, Figure 199, Figure 201, and Figure 202.

After filtering the abnormal cases, the strain gauges sensors have to be balanced to on another. Unfortunately, there is not any automatic way to do that. The best solutions found are to first calibrate the offset of the strain gauge signal by symmetry versus the wind speed and the wind direction. Alternatively, the offset can be found by plotting the strain gauges with respect to the wind direction, and identifying visually the points where the signal is converging to zeros, which corresponds to a nacelle position exactly at 90° from the strain gauge direction angle. This point gives two indications: the X-axis coordinate gives an indication of the position angle of the strain gauge and the Y-axis coordinate gives the offset of the strain gauge. Indeed, this position should be almost null for all wind speed. Precisely, it should be exactly equal to the torque, but it is usually very small in comparison with the other bending moments at a low position on the Power. If on the contrary the strain gauges are located close to the hub, the torque dominates the signal at high wind speed, which prevents of using this method. It is the case for the strain gauges at 55m on the Horns Rev turbine, Figure 33, p.75.

The next step to balance the strain gauges between one another is to scale them to obtain the same order of measurement at the same wind speed and at the corresponding wind direction. One way of doing that is by plotting both strain gauges measurements with respect of the wind speed on top of one another. This gives a good check of unbalanced strain gauges, if one signal is significantly less wide than the other is. The strain gauges signals plotted with respect of the wind speed and the wind direction are presented in the following figures:

- Horns Rev, p.73: Figure 29, Figure 30, Figure 31, Figure 32, and Figure 33.
- Siemens, p.135: Figure 136, and Figure 137.

- Neg Micon, p.154: Figure 170.
- Nordtank, p.173: Figure 203.

After filtering out abnormal cases, calibrating, and balancing the strain gauges signals, the methods presented in section 2.4.4 can be directly used to derive the thrust force of the turbine. Each method has different input variables, which can be directly measured from a sensor (e.g. the wind direction and the wind speed). These variables are derived from different sensors (e.g. the shaft torque derived from the power and the rotation speed, and the air density derived from the air temperature and the air pressure). Otherwise, they can be found in the documentation (e.g. tower height, rotor width). Nonetheless, some elements, like the tilt moment are neglected because of the lack of documentation and sensor measurement (shaft bending moment). Finally, some elements must be guessed from general knowledge because there is not any information available on it (e.g. the rotor bending moment when not measured in the calibration campaign, the tower drag coefficient).

o Necessity of an extra calibration of the strain gauges

In most of the cases observed, the strain gauges are given with proper calibration values obtained during a calibration campaign similar to the one described in section 2.3. The only case where it is needed to correct these calibrations is for the Horns Rev wind turbine. Horns Rev is an offshore wind farm with a limited accessibility, which prevents from doing an accurate calibration campaign. Indeed, fixing a cable on the hub and pulling it at a controlled distance and with a controlled force on a boat is particularly challenging. The calibration available with the data set of Horns Rev does not give a result in accordance with the manufacturer curve and do not make sense in term of the thrust force/energy extraction relationship presented in Appendix A3. The strain gauges signals are scaled in order to obtain the same order of magnitude as the manufacturer BEM curve at low wind speed. This action prevents any comparison on the order of magnitude of the measured thrust curve with respect to the theoretical thrust curve. Nonetheless, it is still possible to do a qualitative comparison on the shape of the curve.

o The results accuracy depending of the different methods

In general, the method 2 gives the lowest amount of scatter in comparison with method 1 and method 3. The only case where it is better to use method 1 is for the Siemens wind turbine, where one of the strain gauge has a shifting offset, which cannot be corrected easily. In that case using only the reliable strain gauge in optimal wind direction with the method 1 is giving significantly better results than using method 2. Method 3, which excludes the wind direction sensor, is in some cases of lower quality than Method 2, probably because of a higher sensitivity of the result with respect to the balance between the strain gauges signals. Furthermore, Method 3 gives frequently negative results because of the problem explained in the previous section. Nonetheless, for very well calibrated strain gauges it seems that it gives a similar result than Method 2, and maybe even less scatter in the case of Nordtank.

- Horns Rev, p.76: Figure 34, Figure 35, Figure 37, Figure 39, Figure 40, Figure 42, Figure 44, Figure 45, Figure 47, Figure 49, Figure 50, Figure 52, Figure 54, Figure 55, Figure 57, and Figure 59.

- Siemens, p.140: Figure 144, Figure 145, and Figure 147.
- Neg Micon, p.155: Figure 171, Figure 172, and Figure 174.
- Nordtank, p.174: Figure 204, Figure 205, and Figure 207.

o Coherence of the met mast sensors with the wind turbine

As it can be expected, the correlation and the coherence of the met mast sensors used with the strain gauges measurements are critical to obtain accurate results. For instance, in the case of Horns Rev, the met masts available are located at several kilometres from the turbine. Therefore, the wind properties measured at the met mast have a poor agreement with the wind properties effectively influencing the wind turbine, and the strain gauges measurements. The direct consequence of using the wind speed and wind direction recorded at the met mast instead of the wind speed measured at the nacelle and the nacelle direction is an increase of the data scatter.

It is important to understand that this increase of scatter is concretely an increase of the type A uncertainty, which is also inversely proportional to the square root of the number of points used to measure the averaged thrust (as explained in Appendix B). Therefore, using the met mast sensors as a source might still be more accurate, in term of combined standard uncertainty, than using the uncalibrated nacelle sensors, which has probably larger type B uncertainties than the met mast sensors. For instance, the nacelle anemometer is known to give biased results in comparison with a met mast, especially at high wind speed where the constant blade pitching modify the inflow characteristics seen by the anemometer.

The case of Horns Rev is unfortunately even more complex, because the wind turbine is operating most of the time in the shadow of other wind turbines affecting significantly the wind properties seen by the turbine as well as the accuracy of the nacelle anemometer. Nonetheless, it was decided to keep the nacelle anemometer and the yaw direction to derive the thrust in order to obtain less scatter in the plots. However, the reader should keep in mind that for wind speed higher than the rated wind speed, the wind speed recorded is probably a bit lower than the one actually seen by the turbine, and therefore the shape of the thrust curve has a steeper slope than it would using a local met mast anemometer.

o Comparison with the manufacturer thrust curve

The thrust curve and thrust coefficient is compared with the one given by the manufacturer, when available (e.g. Horns Rev and Neg Micon). Those curves are in general generated from Blade Element Method (BEM) codes using airfoil data as an input under standard air density conditions and must be scaled to the local air density for comparison.

For tower bottom strain gauges measurements, the resulting thrust curve is in good agreement with the BEM curve. In the case of Horns Rev, what differs is the peak at rated wind speed that can be seen on the BEM curve but not in the measurements (Figure 35, p.77). This peak is coming from the large jump of the theoretical pitch angle derived from the blade element theory (5° on an increment of 1m/s). This pitch control seems to fails to model realistically the behaviour of the turbine at this wind speed: in comparison, the pitch angle measured on the turbine has a significantly smoother increase at this height. The difference might be in part due to the effect of the inflow turbulence on the rotor averaged over a time-period of 10 minutes.

On the other hand, in the case of Neg Micon, the opposite remark can be made: a peak, clearly visible at rated wind speed on the measurement thrust curve, is not present on the manufacturer thrust curve. A similar interpretation can be made as for Horns Rev. Although the data set did not include the airfoil data of the turbines, it can be assumed that the difference between the measured and the manufacturer thrust is coming from a difference in the pitch control mechanism used in the BEM code, and in reality.

While this comparison can hardly be considered, strictly speaking, as a validation of the measurement method proposed or of the manufacturer method for deriving the thrust, the good agreement between the two methods, tends to confirm their respective correctness. Indeed, while both methods (the tower bending moment model and in the blade element method) encompass a fair amount of restrictive assumptions, those assumptions are taken on completely different aspects that have no direct correlation between one another. E.g. the assumption of no tilt moment in the tower bending moment model, and the assumption of no shear forces acting on the control volume in the blade element method.

- **Validity of the model proposed**

Nonetheless, despite the good agreement of the measurement with tower bottom strain gauges with the Blade Element Method result, if the same analysis is carried on with strain gauges located on the upper part of the tower, closer to the nacelle, the resulting thrust curve becomes different.

In the case of Horns Rev, several set up of strain gauges are available at different heights on the tower. For an increasing height on the tower, the resulting thrust curve agreement with the tower bottom strain gauges curve decreases (Figure 59, p.91). Especially, the tower top strain gauges, located at 4 meters from the hub, is also giving a rather poor agreement with the BEM curve (Figure 55, p.89). This fact shows the limits of the model and the assumptions chosen. For instance, the tilt moment is expected to have a significant influence on strain gauges measurement, and by neglecting it, the error introduced becomes more and more important for strain gauges located at high position on the tower, as the magnitude of the bending moment generated by the thrust is reduced. Other elements such as the tower drag bending moment is also expected to introduce errors in high wind speed as the drag coefficient is only guessed and the model does not consider the interaction between the blades rotation and the tower on the upper half of the tower.

It is difficult to estimate the uncertainty of the model, as many parameters are unknown, but it seems fair to say that this uncertainty is in part related with the distance between the strain gauges and the tower top.

2.5 Uncertainty of measurements

The method to derive the combined standard uncertainty is based on the same theory presented in Appendix B2. The function used to model the thrust is one of the 3 methods presented in the previous section. As the goal is to obtain the smallest uncertainty possible, the choice of the method will depend of the accuracy of the different sensors available.

For each 10-minute time series, the standard uncertainty of type *A* of the sensors (if available) is combined with the uncertainty of type *B* to derive the combined standard uncertainty of the corresponding thrust. The combined standard uncertainty of the thrust curve is derived in a similar

way in each bin of wind speed considered. In addition this uncertainty takes also in account the impact of the type *B* wind speed uncertainty.

Because of the limited amount of documentation concerning the different sensors available, the type B uncertainties are difficult to estimate with precision in most cases. They are therefore "guessed" from general knowledge, and from similar sensors documentation, when available. Those uncertainties are intentionally chosen conservative and therefore lead to an over prediction of the combined standard uncertainty of the thrust curve. The results are therefore more focused on the sensitivity of the thrust's combined uncertainty with respect to the different elements uncertainties than on the order of magnitude of the combined uncertainty.

Finally, as it was explained in the previous section, the model's uncertainty is expected to increase with the strain gauge location height on the tower. This uncertainty is not taken into account in the following analysis in spite of its relatively large importance.

2.5.1 The different elements uncertainties

In this section, the standard uncertainty and sensitivity coefficient of each elements of the model are presented.

- The **strain gauges measurements** are analyzed independently, with their respective gain and offset. The gain and the offset standard uncertainty are estimated from the calibration campaign whenever it is possible; otherwise their respective uncertainties are estimated from general knowledge of other similar campaigns. To these standard uncertainties is added the uncertainty of measurement of the strain gauge by itself.

$$\begin{cases} \overline{SG_i} = \overline{Gain_i} \cdot \overline{sg_i} + \overline{Offset_i} \\ u_A{}^2\left(SG_i\right) = \left(\overline{Gain_i} \cdot u_A\left(sg_i\right)\right)^2 \\ u_B{}^2\left(SG_i\right) = \left(\overline{sg_i} \cdot u_B\left(Gain_i\right)\right)^2 + u_B{}^2\left(Offset_i\right) \end{cases} \quad \text{(III-2.19)}$$

Its sensitivity coefficient can be derived for the three methods by differentiating the corresponding equation with respect to the strain gauge, for fixed mean values of the other elements

$$\begin{aligned} c_1\left(SG_i\right) &= \frac{1}{\left(\overline{H_{Hub}} - \overline{H_{SG}}\right) \cdot \cos\left(\overline{\theta_{wind}} - \overline{\alpha_i}\right)} \\ c_2\left(SG_i\right) &= \frac{\sin\left(\overline{\theta_{wind}} - \overline{\alpha_j}\right)}{\left(\overline{H_{Hub}} - \overline{H_{SG}}\right) \cdot \sin\left(\overline{\alpha_i} - \overline{\alpha_j}\right)} \\ c_2\left(SG_i\right) &= \frac{2\overline{SG_i} - \overline{SG_j}\cos\left(\overline{\alpha_i} - \overline{\alpha_j}\right)}{2\sin^2\left(\overline{\alpha_i} - \overline{\alpha_j}\right)\left(\overline{H_{Hub}} - \overline{H_{SG}}\right) \cdot \sqrt{\dfrac{\overline{SG_i}^2 + \overline{SG_j}^2 - 2\overline{SG_i}\,\overline{SG_j}\cos\left(\overline{\alpha_i} - \overline{\alpha_j}\right)}{\sin^2\left(\overline{\alpha_i} - \overline{\alpha_j}\right)} - \overline{BM_{Torque}}^2}} \end{aligned} \quad \text{(III-2.20)}$$

- The **strain gauge position angle** is also to be considered in the derivation of the combined standard uncertainty. If no physical information is given from the strain gauge calibration

campaign, the position is derived from the strain gauge bending moment measurements. The correct position angle is determined by plotting the bending moments in the z direction (so the strain gauges measurement minus the bending moment in the x direction, i.e. the torque contribution) with respect to the wind direction. In each wind direction bins, the average bending moment is computed. The position of the strain gauge is then defined by the maximum bending moment wind direction sector (or more precisely, the wind direction where the mean bending moment is null and adding pi/2).

There is no direct method to quantify the standard uncertainty of the position, if the wind direction is used to find the position angle, the uncertainty in radian can be expressed as the confidence factor divided by square root of 3 (by assuming a rectangular distribution).

The sensitivity coefficients are differentiated from the 3 equations presented in the previous section.

$$
\begin{aligned}
c_1(\alpha_i) &= -\frac{\overline{BM_{Torque}} + \overline{SG_i}\cdot\sin\left(\overline{\alpha_i} - \overline{\theta_{wind}}\right)}{\left(\overline{H_{Hub}} - \overline{H_{SG}}\right)\cdot\cos^2\left(\overline{\alpha_i} - \overline{\theta_{wind}}\right)} \\
c_2(\alpha_i) &= \frac{\left(\overline{SG_i}\cdot\cos\left(\overline{\alpha_i} - \overline{\alpha_j}\right) - \overline{SG_j}\right)\cdot\sin\left(\overline{\alpha_j} - \overline{\theta_{wind}}\right)}{\left(\overline{H_{Hub}} - \overline{H_{SG}}\right)\cdot\sin^2\left(\overline{\alpha_1} - \overline{\alpha_2}\right)} \\
c_3(\alpha_i) &= \frac{\overline{SG_i}\,\overline{SG_j}\left[3 + \cos\left(2\left(\overline{\alpha_i} - \overline{\alpha_j}\right)\right)\right] - 4\left(\overline{SG_i}^2 + \overline{SG_j}^2\right)\cos\left(\overline{\alpha_i} - \overline{\alpha_j}\right)}{4\sin^3\left(\overline{\alpha_i} - \overline{\alpha_j}\right)\left(\overline{H_{Hub}} - \overline{H_{SG}}\right)\cdot\sqrt{\dfrac{\overline{SG_i}^2 + \overline{SG_j}^2 - 2\overline{SG_i}\,\overline{SG_j}\cos\left(\overline{\alpha_i} - \overline{\alpha_j}\right)}{\sin^2\left(\overline{\alpha_i} - \overline{\alpha_j}\right)} - \overline{BM_{Torque}}^2}}
\end{aligned}
\qquad \text{(III-2.21)}
$$

- The **wind direction** sensor plays a role in the two first methods. The standard uncertainty of this sensor can be directly determined using its standard deviation. If the wind direction sensor is located far from the turbine, it becomes necessary to add an uncertainty term related to the geographical coherence between the sensor and the wind turbine. When only the yaw of the turbine is available, the standard deviation of the yaw normalized over the square root of the number of elements in the time series, is used as an uncertainty of type A.

  In general, it is difficult to have a confidence on the wind direction lower than 5°, especially when the sensor used is a yaw direction. The uncertainty of type B is therefore taken in all the cases as (III-2.22), where the square root of 3 is coming from an assumption of a rectangular distribution of the uncertainty.

$$u_B(WD) = \frac{\pi}{\sqrt{3}}\frac{5°}{180°} \qquad \text{(III-2.22)}$$

The sensitivity coefficient for the three methods can be derived by differentiating with respect to the wind direction and taking the mean values for the other elements.

$$\begin{aligned} c_1\left(\theta_{wind}\right) &= -\frac{\overline{BM_{Torque}} + \overline{SG_i}\cdot\sin\left(\overline{\alpha_i} - \overline{\theta_{wind}}\right)}{\left(\overline{H_{Hub}} - \overline{H_{SG}}\right)\cdot\cos^2\left(\overline{\alpha_i} - \overline{\theta_{wind}}\right)} \\ c_2\left(\theta_{wind}\right) &= \frac{\overline{SG_1}\cdot\cos\left(\overline{\alpha_2} - \overline{\theta_{wind}}\right) - \overline{SG_2}\cdot\cos\left(\overline{\alpha_1} - \overline{\theta_{wind}}\right)}{\left(\overline{H_{Hub}} - \overline{H_{SG}}\right)\cdot\sin\left(\overline{\alpha_1} - \overline{\alpha_2}\right)} \\ c_3\left(\theta_{wind}\right) &= 0 \end{aligned} \qquad \text{(III-2.23)}$$

- The **torque** is derived directly from the shaft torsion measurement or from the power divided by the rotation speed of the rotor. The standard uncertainty of the torque is therefore derived accordingly to the method used to derive its mean value. From the standard deviation of the shaft torsion divided by square root of K, the number of elements in the 10-minute time series (typically 600 for a 1Hz acquisition system). It can also be derived from the combined standard uncertainty of the rotation speed and the electrical power output time series.

$$\begin{aligned} u_A\left(BM_{Torque}\right) &= std\left(Torsion_{Shaft}\right)/\sqrt{K} \\ u_B\left(BM_{Torque}\right) &= u_B\left(Torsion_{Shaft}\right) \\ u_A^2\left(BM_{Torque}\right) &= \left[\overline{RotationSpeed}\cdot u_A\left(Power\right)\right]^2 + \left[\overline{Power}\cdot u_A\left(RotationSpeed\right)\right]^2 \\ u_B^2\left(BM_{Torque}\right) &= \left[\overline{RotationSpeed}\cdot u_B\left(Power\right)\right]^2 + \left[\overline{Power}\cdot u_B\left(RotationSpeed\right)\right]^2 \end{aligned} \qquad \text{(III-2.24)}$$

Similarly, as with the other elements, the sensitivity coefficient is derived from the 3 methods equations.

$$\begin{aligned} c_1\left(BM_{Torque}\right) &= \frac{\tan\left(\overline{\alpha_i} - \overline{\theta_{wind}}\right)}{\overline{H_{Hub}} - \overline{H_{SG}}} \\ c_2\left(BM_{Torque}\right) &= 0 \\ c_3\left(BM_{Torque}\right) &= \frac{-BM_{Torque}}{\left(\overline{H_{Hub}} - \overline{H_{SG}}\right)\sqrt{\dfrac{\overline{SG_i}^2 + \overline{SG_j}^2 - 2\overline{SG_i}\,\overline{SG_j}\cos\left(\overline{\alpha_i} - \overline{\alpha_j}\right)}{\sin^2\left(\overline{\alpha_i} - \overline{\alpha_j}\right)} - \overline{BM_{Torque}}^2}} \end{aligned} \qquad \text{(III-2.25)}$$

- The **rotor weight bending moment** can be derived from the strain gauge bending moment when there is no wind acting on the turbine. In that case the strain gauges are influenced only by the gravity. The mean value is obtained by projecting the strain gauge measurement on the nacelle coordinate using the nacelle direction and the strain gauge position angle. At the end the rotor weight bending moment standard uncertainty is dependent of the strain gauge standard uncertainty, the strain gauge standard uncertainty and of the yaw mechanism uncertainty.

$$\overline{BM_{Rotor}} = \overline{\left(\frac{SG_i}{\cos\left(\theta_{wind} - \alpha_i\right)}\right)}$$
$$u^2\left(BM_{Rotor}\right) = \left(\frac{1}{\cos\left(\overline{\theta_{wind}} - \overline{\alpha_i}\right)} u\left(SG_i\right)\right)^2 + \left(\overline{SG_i}\frac{\tan\left(\overline{\theta_{wind}} - \overline{\alpha_i}\right)}{\cos\left(\overline{\theta_{wind}} - \overline{\alpha_i}\right)}\right)^2 \left(u^2\left(\theta_{wind}\right) + u^2\left(\alpha_i\right)\right) \quad \text{(III-2.26)}$$

When the rotor weight bending moment is "guessed" from the thrust curve, the uncertainty of the rotor weight is so big that a type B uncertainty is chosen in proportion with the rotor weight bending moment.

The sensitivity coefficient (found as usual by differentiating the methods equations) is simply minus one divided by the distance between the strain gauge position and the hub height, for all methods.

$$c_1\left(BM_{rotor}\right) = c_2\left(BM_{rotor}\right) = c_3\left(BM_{rotor}\right) = \frac{-1}{\overline{H_{Hub}} - \overline{H_{SG}}} \quad \text{(III-2.27)}$$

- The **tilt moment** can be derived from the shaft bending moment projected on the fixed nacelle coordinates, by subtracting the rotor weight bending moment. The type A standard uncertainty is then the standard deviation of the 10-minute time series divided by the square root of the number of information, if it is available. The type B uncertainty is probably trickier to determine as it has to take the azimuthal position sensor uncertainty into consideration.

  As for the tower bottom strain gauge, the uncertainty of the gain and offset should also be considered in the same way. The sensitivity coefficient is exactly the same as the rotor weight bending moment.

  In practice, the shaft bending moment is rarely available, and the only one available for this analysis (i.e Siemens data) has a shifting offset which made it impractical to use. The tilt moment is therefore neglected in al l the cases.

- The **tower drag bending moment** is derived from the tower drag force model presented in section 2.4.2 . The combined standard uncertainty of the tower drag force is therefore a function of the hub height H_{Hub}, the strain gauge height H_{SG}, the wind speed U, the drag coefficient C_D, the density ρ, and the top and bottom radius R_{Hub}, and R_0. For each element of this equation, the equation is differentiated with respect to the corresponding element and multiplied by its standard uncertainty. All the elements, except the wind speed are type B uncertainties and are found from the documentation of the tower geometry, or on the strain gauge position documentation. If they are missing, a general order of magnitude is used. The sensitivity coefficient of the tower drag bending moment is the same as the sensitivity coefficient of the rotor weight bending moment and the tilt bending moment.

$$\overline{BM_{Tower}} = \overline{\frac{1}{12 H_{Hub}} \cdot \pi \rho C_D U^2 \left(H_{Hub} - H_{SG}\right)^2 \left(H_{Hub}\left(2R_{Hub} + R_0\right) + H_{SG}\left(R_{Hub} - R_0\right)\right)} \quad \text{(III-2.28)}$$

$$
\begin{aligned}
u_A^2\left(BM_{Tower}\right) &= \left[\frac{u_A(U)}{6\overline{H_{Hub}}}\cdot\pi\,\overline{\rho}\,\overline{C_D}\,\overline{U}\left(\overline{H_{Hub}}-\overline{H_{SG}}\right)^2\left(\overline{H_{Hub}}\left(2\overline{R_{Hub}}+\overline{R_0}\right)+\overline{H_{SG}}\left(\overline{R_{Hub}}-\overline{R_0}\right)\right)\right]^2 \\
u_B^2\left(BM_{Tower}\right) &= \left[\frac{u_B(U)}{6\overline{H_{Hub}}}\cdot\pi\,\overline{\rho}\,\overline{C_D}\,\overline{U}\left(\overline{H_{Hub}}-\overline{H_{SG}}\right)^2\left(\overline{H_{Hub}}\left(2\overline{R_{Hub}}+\overline{R_0}\right)+\overline{H_{SG}}\left(\overline{R_{Hub}}-\overline{R_0}\right)\right)\right]^2 \\
&+\left[\frac{u_B(C_D)}{12\overline{H_{Hub}}}\cdot\pi\,\overline{\rho}\,\overline{U}^2\left(\overline{H_{Hub}}-\overline{H_{SG}}\right)^2\left(\overline{H_{Hub}}\left(2\overline{R_{Hub}}+\overline{R_0}\right)+\overline{H_{SG}}\left(\overline{R_{Hub}}-\overline{R_0}\right)\right)\right]^2 \\
&+\left[\frac{u_B(\rho)}{12\overline{H_{Hub}}}\cdot\pi\,\overline{C_D}\,\overline{U}^2\left(\overline{H_{Hub}}-\overline{H_{SG}}\right)^2\left(\overline{H_{Hub}}\left(2\overline{R_{Hub}}+\overline{R_0}\right)+\overline{H_{SG}}\left(\overline{R_{Hub}}-\overline{R_0}\right)\right)\right]^2 \\
&+\left[\frac{u_B(H_{Hub})}{12\overline{H_{Hub}}^2}\cdot\pi\,\overline{\rho}\,\overline{C_D}\,\overline{U}^2\cdot\left(2\overline{H_{Hub}}^3\left(2\overline{R_{Hub}}+\overline{R_0}\right)+\overline{H_{SG}}^3\left(\overline{R_{Hub}}-\overline{R_0}\right)-3\overline{H_{SG}}\cdot\overline{H_{Hub}}\left(\overline{R_{Hub}}+\overline{R_0}\right)\right)\right]^2 \\
&+\left[\frac{u_B(H_{SG})}{4\overline{H_{Hub}}}\cdot\pi\,\overline{\rho}\,\overline{C_D}\,\overline{U}^2\left(\overline{H_{Hub}}-\overline{H_{SG}}\right)\left(\overline{H_{Hub}}\left(\overline{R_{Hub}}+\overline{R_0}\right)+\overline{H_{SG}}\left(\overline{R_{Hub}}-\overline{R_0}\right)\right)\right]^2 \\
&+\left[\frac{u_B(R_{Hub})}{12\overline{H_{Hub}}}\cdot\pi\,\overline{\rho}\,\overline{C_D}\,\overline{U}^2\left(\overline{H_{Hub}}-\overline{H_{SG}}\right)^2\left(2\overline{H_{Hub}}+\overline{H_{SG}}\right)\right] \\
&+\left[\frac{u_B(R_0)}{12\overline{H_{Hub}}}\cdot\pi\,\overline{\rho}\,\overline{C_D}\,\overline{U}^2\left(\overline{H_{Hub}}-\overline{H_{SG}}\right)^3\right]^2
\end{aligned}
\qquad \text{(III-2.29)}
$$

- The **wind speed** is measured whether at the turbine, by interpolation of the power using the power curve to derive the wind speed, or by using the nacelle anemometer with an empirical correction; or whether at a met mast located nearby the turbine. The type *A* standard uncertainty of the wind speed may therefore come from the power using the standard deviation of the power divided by an empirical coefficient *B* and the slope of the power curve *dP/dU* as suggested by Barthelmie et al. [2006] (III-2.30), or directly from an anemometer through its standard deviation of the 10-minutes considered.

$$\sigma_P = B\,\sigma_u\left(\frac{dP}{dU}\right)_u \qquad \text{(III-2.30)}$$

The two formulations of the standard uncertainty of wind speed are therefore

$$
\begin{aligned}
u_A(U) &= std(U)/\sqrt{K} \\
u_A(U) &= \frac{1}{\sqrt{K}}\frac{std(P)}{B\left.\frac{dP}{dU}\right|_u}
\end{aligned}
\qquad \text{(III-2.31)}
$$

The type B uncertainty of wind speed measurement has been extensively described in the IEC standard dealing with resource assessment and power measurement [IEC61400-12]. A simpler estimation is used here by taking a confidence interval of +/-0.5m/s to +/-1m/s in order to simplify the amount of assumptions. Ideally, all the parameters should be taken into account to assess the wind speed uncertainty, as it was proved to be one of the major sources

of uncertainty in the thrust. However, due to the general lack of information concerning the calibration of the anemometers, or due to the limitations of using a nacelle anemometers, a larger level of confidence is preferred. According to the *Guidelines for Design of Wind Turbines* [DNV/Risø, 2002], it is advised to take the uncertainty in wind speed as 2-3% of the wind speed value. In the present case the wind turbine is often in the wake of other turbines, and the nacelle anemometer used in most cases are greatly influenced by the blade shadow. So a significantly larger confidence interval seems more appropriate.

After the computation of each elements standard uncertainty, and their corresponding sensitivity coefficients, the combined standard uncertainty of the thrust can be derived by summing the different elements. As in equation (III-2.32), where N is the number of element X_i in the equation k of the thrust, with $c_k(X_i)$ their corresponding sensitivity coefficient, $u(Xi)$ their corresponding standard uncertainty.

$$u^2\left(Thrust_k\right) = \sum_{i=1}^{N}\left[c_k\left(X_i\right)u\left(X_i\right)\right]^2 \tag{III-2.32}$$

2.5.2 The combined standard uncertainty

At this point, the combined standard uncertainty of each 10-minute average thrust is known. In order to derive the thrust curve with respect to the wind speed, the 10-minute average values will be gathered into wind speed bins and then averaged over each bin. The standard method to follow is to derive the type A standard uncertainty of the thrust from the standard deviation of the thrust in each bin, and to divide it by the square root of the number of element in the bin. This division comes from the *Central Limit Theorem* described in Appendix B, which states that the standard uncertainty of the mean of N means from independent samples with the same probability density is the standard deviation of the means divided by the square root of the mean.

$$\boxed{u^2\left(T\left(WS_i\right)\right) = \frac{1}{N\left(N-1\right)}\sum_{n=1}^{N}\left(\overline{T}-T_n\right)^2 + \sum_{n=1}^{N}u_B^2\left(\overline{X}_n\right)} \tag{III-2.33}$$

However, this method does not to take into account the uncertainty of the wind speed used to gather the thrust data into different bins. Indeed, a very poor wind speed sensor, even with the best accuracy possible on the thrust will not produce an accurate thrust curve.

So in order to take into account the uncertainty of wind speed on the x-axis of the plot, the standard uncertainty of the wind speed sensor is multiplied by a sensitivity coefficient and is added to the final uncertainty of the thrust.

The problem is finally to define properly the sensitivity coefficient of the wind speed. It cannot be derived directly from a model, as the turbine thrust does not have an equation that fully describes it, so it must be calculated numerically using the slop of the thrust curve. This can be done using the equation (IV-1.3) presented in Appendix B4. So by computing the equivalent change of thrust to an increase of wind speed from $U-u(U)$ to $U+u(U)$.

$$c\left(U\right) = \left|\frac{Thrust\left(U+u\left(U\right)\right) - Thrust\left(U-u\left(U\right)\right)}{2u\left(U\right)}\right| \tag{III-2.34}$$

2.5.3 Results

The results are presented for each data set in the appendices.

Horns Rev, p.77: Figure 35, Figure 36, Figure 37, Figure 38, Table 7, and Table 8.

Siemens, p.141: Figure 145, Figure 146, Figure 147, Figure 148, Table 10, Table 11, and Table 12.

Neg Micon, p.156: Figure 172, Figure 173, Figure 174, Figure 175, and Table 16.

Nordtank, p.175: Figure 205, Figure 206, Figure 207, Figure 208, Table 19, and Table 23.

The standard uncertainty of each element is presented in the tables in introduction of the results. The combined uncertainty is plotted together with the thrust and thrust coefficient and is also given in the tables. Furthermore, some extra plots represent the "uncertainty contribution" of each element to the final thrust expression. In these plots, each layer accounts for each element that contributes to the combined standard uncertainty. The values plotted are the standard uncertainty of type A or B multiplied by their corresponding sensitivity coefficient and divided by the value of the thrust. Therefore, the sum of all the layers is not equal to the combined standard uncertainty. Instead, the combined standard uncertainty is defined as the root sum square of all these values. The information given by these plots is therefore more on the evolution of the influence of each element with respect to the wind speed.

The measurements are giving the same picture concerning each element's contribution to the combined standard uncertainty of the measurement of the thrust. The two most influent elements, in term of uncertainty, are the type B wind speed uncertainty and the type B strain gauges uncertainty. The rotor mass moment and the tower drag moment give also quite important contribution to the combined uncertainty at low and high wind speed respectively. It is quite interesting to see that the wind direction, even with a rather large uncertainty (a confidence interval of +/-10°) has a relatively limited influence over the final uncertainty in method 2. On the other hand, method 1, which uses only on strain gauge, relies much more on the wind direction sensor and the uncertainty is therefore increased (see Siemens cases). Finally, even if the scatter of the data seems sometimes important, the contribution of the type A uncertainty of the thrust is considerably smaller than the other type B uncertainties.

Different additional scenarios of input uncertainties are considered and compared for each data set in Appendix C:

Horns Rev, p.92: Figure 60, Figure 61, Figure 62, Figure 63, Figure 64, and Figure 65.

Siemens, p.144: Figure 149, Figure 150, Figure 151, Figure 152, Figure 153, and Figure 154.

Neg Micon, p.158: Figure 176, Figure 177, Figure 178, and Figure 179.

Nordtank, p.177: Figure 209, Figure 210, Figure 211, Figure 212, Figure 213, and Figure 214.

The results show as expected a great variation of the combined uncertainty with respect to the input uncertainties chosen. On the other hand, the trend of the combined uncertainty with respect the wind speed is in most cases unchanged. For very optimistic scenario the combined standard uncertainty of the thrust is in most cases around 4-8% of the thrust and thrust coefficient value.

While this uncertainty order of magnitude is probably reached for the very precise calibration campaigns carried on in the cases of Nordtank, Siemens and Neg Micon, the data set of Horns rev as a probably much larger combined uncertainty.

2.6 Parameter study

The resulting strain gauges thrust curves are plotted with respect to different parameters to detect any visible correlation. A statistical analysis of the correlation coefficient between the thrust and the parameter signal is also possible, but is less interesting qualitatively than plotting, as it does not give any information on how the thrust and the parameters are related.

The comparison of the thrust curve with the wind direction is especially interesting to study because it gives a good check to see if the strain gauges gain, offset and direction angle are correctly balanced between one another and with the wind direction sensor (see Figure 73, Figure 158, Figure 187, and Figure 221 in Appendix C). Similarly, comparing the thrust curve with a time indicator is a good idea to detect any sign of "shifting offset" (when the offset of a strain gauge is changing significantly with the time). In several cases during the data analysis (see Siemens cases in Appendix C3), some strain gauges presented a non-negligible shifting offset, which could not be corrected.

The air density is clearly related with the thrust (see Figure 74, Figure 159, and Figure 188 in Appendix C), as it can be expected, the more dense is the air, and the more force is felt by the turbine for a given wind speed. This is of course why the thrust coefficient is divided, among other parameters, by the air density. The air pressure, and the air humidity can also sometimes give different trends, but these effects are probably related to the air density. The air temperature, is also sometimes giving significant correlations, but it is unclear if this is due to the relationship with the air density or if it is due to the sensitivity of the strain gauge precision with respect to the temperature.

There is a visible trend relating the inflow turbulence intensity with the thrust curve for the Nordtank turbine (see Figure 222, p.184). The thrust curve's slope becomes increasingly steeper for high inflow turbulence intensity (>20%). Unfortunately, the other data sets where this effect could also be studied (Neg Micon and Siemens data) contain mostly low turbulence intensity cases, it is therefore unclear if this dependency regarding the turbulence intensity is related to the stall regulated control or not.

2.7 Conclusion and future work

Three methods to estimate the thrust from bending moments, measured on the tower, are proposed. The results are in good agreement with the thrust curves given by the manufacturer. In addition, these methods give an estimate of the combined uncertainty of the thrust curve. As it is presented in Chapter II, this uncertainty is an important missing indicator for designing more accurate wake losses models. The combined uncertainty is depending on the input uncertainties of each sensor. Without an accurate knowledge of these values, the combined uncertainty of the thrust can only be "guessed". Therefore, in order to obtain a more accurate estimation of the thrust uncertainty, it is advised to estimate and document the type B uncertainty of each sensors used

during the measurement campaign. Due to the complexity of estimating the thrust curve and its uncertainty, there is a need for a standard method in the same manner as there is a standard method for measuring the power curve.

The strain gauges measurements showed that for and increasing height on the tower the difference between the estimated thrust curve and the one given by the manufacturer is increasing. This observation shows that the model presented relies on assumptions (e.g. neglecting the tilt moment, the tower drag model) that becomes increasingly unrealistic. Therefore, there is a need for more work on this matter to obtain a model independent of the strain gauges height.

3 Estimation of the thrust force using the BEM theory

The steady BEM theory, which is succinctly introduced in Appendix A, is applied using real turbine airfoil data to compare the estimate C_T curve from the BEM theory with the one measured using strain gauges, and the one given by the manufacturer. Finally, the uncertainty of the results is discussed.

The Steady Blade Element Method used in this section is presented in a book by Martin O.L. Hansen [Hansen, 2000], and was created during a course he taught, "Wind Turbine Technology and Aerodynamics", at the Technical University of Denmark (DTU). As there is not any essential modification done on the algorithm, the whole method is not presented in this thesis.

3.1 Results

In order to study the realism of the steady blade element code developed, the final thrust curve is compared with tower bending moment measurements and the manufacturer thrust curves.

In the only case where the airfoil data are available (Horns Rev wind turbines), the manufacturer thrust curve is known to be derived from a similar blade element code, but with a rather more complicated pitch mechanism. The idea of this comparison is not to propose a complete realistic simulation of a wind turbine but more to estimate the thrust from measurements, and therefore the pitch and the rotation speed are directly measured from the real data available.

The strain gauges signal of the wind turbine, where the airfoil data are known (Horns Rev), are not correctly calibrated, and while the offset can be corrected with a quite good accuracy (by symmetry with respect to the wind direction), the gain cannot be estimated independently from the thrust. In order to determine the gain, the only solution found is to scale it with respect to the manufacturer C_T. Therefore, the comparison makes only sense in term of curve shape, and not in term of order of magnitude.

The results are giving much less scatter than the thrust estimated using the strain gauges, with a good agreement on the mean value with the manufacturer C_T curve (see Figure 80, p.103). Of course, as the gains of the strain gauges are scaled, the only point of comparison is concerning the difference of shape.

On the contrary, the power curve measured and estimated from the blade element theory are slightly different (see Figure 79, p.102). The estimated power using the blade element theory is significantly higher for all wind speeds. The difference can be in part explained by the electrical losses taking place in the generator, as well as the mechanical losses in the gearbox.

At low wind speed, the BEM thrust curve has a very low data scatter in comparison with the strain gauges measurements. This is an expected result, as the strain gauges are largely influenced by the structural vibrations of the tower, which create necessarily a rather high variance in the

measurements. In contrary, the blade element method is relying on sensors that are relatively independent from structural vibrations. Nonetheless, at high wind speeds, the data scattering seems to be of the same order of magnitude for both way of deriving the thrust. The pitch and the rotation speed signals do not reflect the same amount of scatter, so the explanation is somewhere else. It seems acceptable to say that the scatter of the BEM thrust is at least partly related with the scatter in power observed at high wind speeds. One explanation could come from the generator, which can partly control a quantity of power extracted, by controlling its slip. If not all the power is extracted, part of the unused energy is stored in the rotation speed of the rotor, which will be used later on when the wind speed will have decreased. These phenomena create some unbalance between the wind speed and the power extraction, which might partly explain the scatter in power and in thrust compared with the measurements.

Another important detail is the difference at high wind speeds between the BEM thrust curve and the manufacturer thrust curve. The peak at 12-13m/s is probably due to the pitch control mechanism, as it is explained in section 2.4.5 . For higher wind speed, the slopes of the measured thrust curves (both blade element and strain gauges) are significantly steeper than the slope of the manufacturer thrust curve. This could be explained by the wind speed sensor used. Indeed, there is no met mast at a close distance from the wind turbine to measure the wind speed and wind direction. The wind speed is therefore recorded at the nacelle anemometer, which is known to under estimate the wind speed for high wind speed.

3.2 Combined uncertainty

In this method, the uncertainties are composed of the input uncertainties (e.g., rotation speed sensor, wind speed sensor, pitch sensor, density, airfoil data) and of the uncertainties of the model. As these last ones are extremely complex, the study will be focused on the input uncertainties. Using the GUM method described in Appendix B, the type A and type B uncertainties can be combined to estimate the combined standard uncertainty of the thrust. The uncertainty of type A of the thrust is derived from the standard deviation of the thrust and divided by the square root of the number of data in the bin (III-3.1). The type B uncertainty of the thrust is the root sum square of the uncertainties of the inputs multiplied by their sensitivity coefficients (III-3.2). Because the blade element method uses a table lookup and an iterative process, the sensitivity coefficients cannot be derived analytically and are therefore derived numerically using the method presented in Appendix B.

$$u_A^2\left(\overline{T}_i\right) = \frac{1}{N\left(N-1\right)}\sum_{j=1}^{N}\left(\overline{T}_i - T_{ij}\right)^2 \tag{III-3.1}$$

$$u_B^2\left(\overline{T}_i\right) = z_B^2\left(\overline{\Omega}_i\right) + z_B^2\left(\overline{\Theta}_i\right) + z_B^2\left(\overline{V}_i\right) + z_B^2\left(\overline{\rho}_i\right) + z_B^2\left(\overline{C}_{Li}, \overline{C}_{Di}\right) \tag{III-3.2}$$

The case of Horns Rev is particularly inadequate to carry on an uncertainty analysis: the wind turbine is located offshore in extreme weather conditions, which may have a significant influence over the sensor's accuracy (e.g., temperature, humidity, salt). Furthermore, the instruments were installed several years prior to the measurement campaign, and might have suffered from corrosion. Finally, the met masts available are located far from the turbines and the turbine is operating most of the time under the wake of other turbines. This situation is yields that there is no accurate way to

determine the wind speed and the wind direction seen by the turbine. Therefore, the uncertainty of each element can only be "guessed" (see Table 1). Therefore, it would be interesting to carry on a similar analysis on a wind turbine with a much more controlled instrumentation.

Table 1: Input uncertainties used

Rotor rotation speed	+/- 10 RPM
Density	+/- 0.05kg/m^3
Pitch angle	+/- 1°
Wind speed	+/- 0.5 m/s
Airfoil data	+/- 5%

The combined uncertainty seems to be significantly reduced in comparison with the strain gauges thrust curve (see Figure 81, p.103). This reduction comes from the decrease of data scatter at low wind speed and the lower number of input sensors. Especially the strain gauge sensors, which have a major influence on the uncertainties of the strain gauge thrust curve, are not needed in this method.

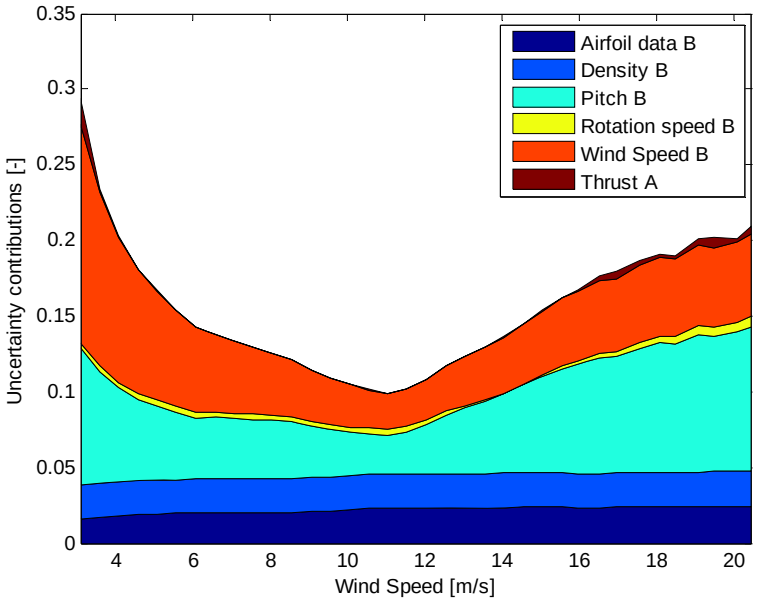

Figure 18: <u>Linear</u> addition of the uncertainty contributions to the thrust in the BEM (using as uncertainty input: $u(\Omega) = \pm 10\,RPM$, $u(\rho) = \pm 0.05\,kg/m^3$, $u(Pitch) = \pm 1°$, $u(WS) = \pm 0.5 m/s$, and $u(Airfoil) = \pm 5\%$). The different colors represents the different components (with their corresponding type A or B uncertainties) considered in the computation of the combined uncertainty of the thrust.

Figure 18 shows the uncertain components the simulation using the blade element method. Each value is an "uncertainty contribution", i.e. the standard uncertainty of the component multiplied by the sensitivity coefficient, and divided by the mean thrust. They are therefore dimension less, and are added at the very end of the computation in a root sum square manner like it is presented in Appendix B.

The main contribution of uncertainty (for this input of uncertainty at least) seems to come from the pitch and wind speed sensors. While 1° and 0.5m/s seems to be a fair boundary for that kind of sensors, the resulting contribution shows that the pitch and the wind speed proportion in the total uncertainty is relatively high. The air density (with 0.05kg/m^3) and the airfoil data (with 5%) plays also an important role in the combined uncertainty, while the rotation speed influence and the random errors have a lower influence. It is interesting to notice that the airfoil data, even with a rather large interval of confidence (+/-5%) is not giving a so large uncertainty on the thrust.

3.3 Conclusion

The good results of this method confirm the fact that the blade element method gives a rather accurate picture of the thrust force applied on the rotor. The level of accuracy is by far the best that could be reached in comparison with the other methods presented, if one neglects the uncertainty of the model itself. This uncertainty is nonetheless of importance, and is coming from the assumptions made in the actuator disc theory and further on, in the blade element theory, as well as the empirical corrections used to palliate the lack of realism of the assumptions (Prandtl's tip –loss factor, Glauert's correction for high values of a…).

Ideally, though, the blade element method should be compared with a properly calibrated wind turbine in order to be able to compare also the order of magnitude of the force. Indeed, by scaling the strain gauge gain to match the BEM thrust, the comparison looses a very important dimension.

Conclusion and future work

In the first chapter, a relationship between the thrust of a wind turbine and the properties of the wake it generates is derived. This relationship is used in the second chapter to stress the importance of the accuracy of estimating the thrust in the context of a growing wind energy industry. The third chapter presents three different methods to estimate the thrust of a wind turbine from measurements. While the first one, based on wake measurements, does not give satisfying results in term of robustness, the general agreement of the results with the two other methods validates the relationship derived in the first chapter. The second method, based on strain gauges measurements, gives satisfying results both in term of order of magnitude and in term of shape of the curve. Nonetheless, the resulting thrust curves are still far too dependent of the distance between the strain gauges and the hub height, which stress the limit of the assumptions taken and the need for more developed models. Finally, the third method is using a very simple blade element code together with the measurement of the pitch sensor and the rotation speed sensor to estimate the thrust. The results are giving a very low amount of scatter in comparison with the strain gauges measurement and globally the same shape.

The results of the different methods roughly agree on the order of magnitude and the shape of the thrust curve. However, a lot of work remains to be done to obtain robust methods to estimate the thrust from measurements. A complete campaign of measurements (both loads and wake), including a precise calibration of the sensors and a documentation of their respective type B uncertainty, would give a more accurate comparison of the different methods, and could be use to refine the models. Ultimately, these methods should be the subject of international standards so that the combined standard uncertainty of the measured thrust could be used in programs estimating the wind parks power production and lifetime. In term, this would give more optimized wind park layout as well as facilitate the risk assessment of the investments in wind energy. Therefore, this could converge to a reduction of the price of wind park projects.

References

Ainslie, J.F. (**1988**), *Calculating the flowfield in the wake of wind turbines*, Journal of Wind Engineering and Industrial Aerodynamics, 27, p. 213-224.

Antoniou, I. (**2003**), *Wind Turbine Test NEG-Micon NM80/2750 Structural loads*, Risø-I-1896(EN). (Not publicly available).

Balling, C. (**2006**), *Calibration 2 of structural load channels, 2.3 MW mkII*, Siemens internal report M-2300-28, rev.03 20.03.2006. (Not publicly available).

Barthelmie, R.J. (**2006**), Frandsen, S.T., Nielsen, N.M., Pryor, S.C., Rethore, P.E., Jørgensen, H.E., *Modeling and measurements of power losses and turbulence intensity in wind turbine wakes at Middelgrunden offshore wind farm.* Wind Energy, WE-06-0045. (to be published).

Burton, T. (**2001**), Sharpe D., Jenkins N., Bossanyi E., *Wind energy handbook,* John Wiley & Sons, ISBN-0-471-48997-2.

Corten, G.P. (**2001**), *Flow separation on wind turbine blades,* PhD thesis, Univ. Utrecht, ISBN 90-393-2582-0.

DNV/Risø, (**2002**), *Guidelines for design of wind turbines, 2nd Ed*, ISBN 87-550-2870-5.

Frandsen, S.T. (**2005**), *Turbulence and turbulence-generated structural loading in wind turbine clusters*, Risø-R-1188(EN).

Hansen, M.O.L (**2000**), *Aerodynamics of wind turbines*, James & James, ISBN-1-902916-06-9.

Glauert, H. (**1935**), *Airplane Propellers, Aerodynamic Theory*, edited by W. F. Durand, J. Springer, Berlin.

IEC61400-12, (**2003**), *Wind turbines - Part 121: Power performance measurements of grid connected wind turbines, 2nd Ed.* International Electro-technical Commission (IEC).

ISO (**1993**), *Guide to expression of uncertainty in measurements (GUM), 1st Ed*, International Organisation for Standardization (ISO), ISBN 92-67-10188-9.

Iotech, *Strain gauge handbook*, http://www.iotech.com/handbook/

Jensen, L.E. (**2006**), *internal memo*, Elsam Eng. (Not publicly available).

Kuik, G.A.M. van (**2003**), *An inconsistency in the actuator disc momentum theory*, Wind Energy, 2003, 7, p.9-19.

Kundu, P., Cohen, I. (2002), *Fluid Mechanics, 2nd Ed*, Elsevier Science. ISBN 0-12-1782514.

Matlab Help, *Curve fitting toolbox*

Medici, D. (**2006**), *Experimental studies of wind turbine wakes – Power optimization and meandering*, PhD thesis, Royal Institute of Technology, Sweden.

Mutlu Summer, B. (**2006**), *Lecture notes on turbulence*, MEK department, Technical University of Denmark (DTU).

Paulsen, U.S. (**2006**), *internal memo*, Risø. (Not publicly available).

Risø (**2001**), *European Wind Turbine Testing Procedure Developments, Task 1: Measurement Method to Verify Wind Turbine Performance Characteristics*, Risø-R-1209(EN).

Sharpe, D.J. (**2004**), *A general momentum theory applied to an energy-extracting actuator disc*, Wind Energy, 2004, 7, p.177–188.

Vermeer, L.J., Sørensen, J.N., Crespo, A. (**2003**), *Wind turbine wake aerodynamics*, Progress in Aerospace Sciences 39 (2003) 467–510.

White, F.M. (**2001**), *Fluid mechanics, 4th Ed*, Mc Graw-Hill, ISBN-0072402172.

Wikipedia, Central Limit Theorem, http://en.wikipedia.org/wiki/Central_limit_theorem/

Wolfram Research, Central Limit Theorem, http://mathworld.wolfram.com

Appendix A
Actuator disc theory

A1 Assumptions

The actuator disc theory introduced by Froude at the end of the XIXth century and extended by Lanchester, Betz and later Glauert has a similar approach to analyze the flow and forces interaction in a wind turbine system as the basic laws of conservation, but using different assumptions over the control volume [Burton, 2001].

Here, the definition of the control volume does not allow any flow transfer through the side faces. The flow is therefore entering through the inflow face, and leaving only through the outflow face. A direct consequence of this is, as the flow downstream the turbine is on average slower than upstream, the area of the outflow face must be bigger than the area of the inflow face in order to satisfy the law of mass conservation ($A_\infty \overline{U_\infty} = A_w \overline{U_w}$).

Another assumption is that there is not any force applied on the side face of the control volume. This particular assumption was analyzed extensively by G. van Kuik [2003] where he demonstrated that this is introducing some inconsistency with the results from the momentum theory; he also introduced the concept of edge forces acting on the actuator disc. The actuator disc theory, under this assumption, is nonetheless widely used in the wind energy world through the blade element method introduced by Glauert [1935] or computational fluid dynamic methods. Because of its limitation an increasing number of semi empirical corrections are applied to produce more realistic results.

Because of these assumptions, the actuator disc theory can only be applied at a relatively short distance from the wind turbine. Indeed, the assumption that the undisturbed flow outside the control volume has no influence over the wake flow can only make sense on a small area downstream the turbine, and become increasingly unrealistic with an increasing distance from the turbine.

A2 Basic results

The basic results of the actuator disc theory are well documented [E.g., Hansen, 2000; Burton, 2001; Sharpe, 2004] and will therefore be quickly presented as an help to understand the results presented in Chapter II.

The actuator disc is considered to be a homogenous permeable disc, on which surface forces are applied continuously. These surface forces, together with the condition of continuity over the flow velocity yield a jump of pressure from p^+ to p^- at the surface of the actuator disc. This pressure increases upstream the turbine, causes the approaching air to slow down from the undisturbed inflow speed U_∞ to $U_\infty(1-a)$ at the disc surface, where a is the so-called axial induced velocity

factor. Immediately after the disc, the pressure will be lower than the ambient pressure $p_\infty > p^-$ and will increase gradually as the flow is proceeding downstream to the turbine to reach its atmospheric value. This increase of pressure will generate another decrease of wind speed to $U_\infty(1-b)$, with $b>a$.

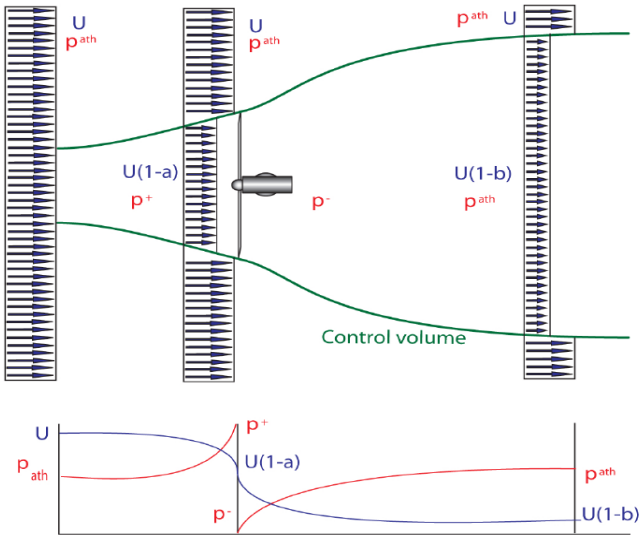

Figure 19: Idealized actuator-disc and control volume

Applying the momentum conservation to this control volume gives simpler results than on the cylindrical control volume. The thrust force is simply the difference of momentum between the inflow momentum, $\dot{m}U_\infty$ and the outflow momentum, $\dot{m}U_\infty(1-b)$.

$$T = \dot{m}\left(U_\infty(1-b) - U_\infty\right) = -b\,\dot{m}U_\infty \tag{III-4.1}$$

The momentum equation can also be applied using the actuator disc control volume, so that the thrust and the pressure difference at the surface of the disc is equal to the difference of momentum at the surface. Because of the continuity, this difference is null, which gives an expression of the thrust related to the pressure difference.

$$T + \left(p^- - p^+\right)A_T = \dot{m}\left(U_\infty(1-a) - U_\infty(1-a)\right) = 0 \tag{III-4.2}$$

$$T = \left(p^+ - p^-\right)A_T \tag{III-4.3}$$

Using the Bernoulli equation for incompressible flow on a streamline between the inflow face and the actuator disc, and between the disc and the outflow face, a relationship between the pressure difference and the axial induction factor b can be derived (III-4.4).

$$\left.\begin{aligned} p_\infty + \frac{1}{2}\rho U_\infty^2 &= p^+ + \frac{1}{2}\rho U_\infty^2 (1-a)^2 \\ p_\infty + \frac{1}{2}\rho U_\infty^2 (1-b)^2 &= p^- + \frac{1}{2}\rho U_\infty^2 (1-a)^2 \end{aligned}\right\} \Rightarrow p^+ - p^- = \frac{1}{2}\rho U_\infty^2 b(b-2) \qquad \text{(III-4.4)}$$

By combining equation (III-4.1), (III-4.3) and (III-4.4), and defining the massflow as the total mass flow going through the actuator disc $\dot{m} = \rho A_T U_\infty (1-a)$, a relationship between *a* and *b* can be derived as (III-4.6).

$$T = A_T \left(p^+ - p^-\right) = \frac{1}{2} A_T \rho U_\infty^2 b(b-2) = -\rho A_T U_\infty^2 (1-a) b \qquad \text{(III-4.5)}$$

$$b = 2a \qquad \text{(III-4.6)}$$

This result establishes that the wind speed decrement is two times bigger in the wake than at the disc surface. It also shows the limits of validity of the actuator disc theory: if $a>½$, the wake wind speed becomes negative.

A3 Thrust and Power relationship

From equation (III-4.5), the thrust coefficient is simply derived as a function of the axial induced velocity (III-4.7) [Hansen, 2000]

$$C_T = 4a(1-a) \qquad \text{(III-4.7)}$$

The power extracted by the turbine can be found using the conservation of energy on the control volume. [Hansen, 2000]

$$P_{Ext} = \frac{1}{2} U_\infty^2 (1-2a)^2 \dot{m} - \frac{1}{2} U_\infty^2 \dot{m} \qquad \text{(III-4.8)}$$

$$P_{Ext} = -2\rho A_T a (1-a)^2 U_\infty^3 \qquad \text{(III-4.9)}$$

The power extracted by the turbine is of course here not only the electrical power generated by the turbine, but also all the additional energy losses associated with the extraction. As the current control volume takes into account only the flow going through the rotor disc, it does not take into account the energy losses of the flow outside the control volume. The approach, and the result, is therefore different from the previous method where the control volume took into account all the flow around the wind turbine.

It is then easy to derive the power coefficient (III-4.11)

$$C_P = \frac{-Power}{\frac{1}{2}\rho A_T U_\infty^3} \qquad \text{(III-4.10)}$$

$$C_{P_{Ext}} = 4a(1-a)^2 \qquad \text{(III-4.11)}$$

The thrust and power coefficients are plotted together on Figure 20. Practically, Lock and later on Glauert measured that for turbulent wake state or heavily loaded actuator disc, at induced velocity higher than one third (*a>1/3*), the thrust coefficient is becoming higher than the one predicted by the actuator disc theory, and can even be higher than one, for induced velocities higher than one half. In that case, the actuator disc theory is not valid anymore, and the power coefficient cannot be estimated analytically. Indeed, for very high thrust, the drop of pressure in the wake becomes so great that it attract momentum from the outflow, which is assumed wrong in the actuator disc theory. [Burton et al., 2001; Sharpe 2003]

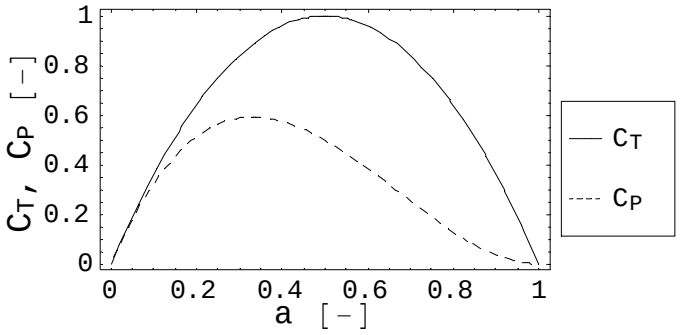

Figure 20: C_T and C_P as a function of the induced velocity

Using equation (III-4.7) and (III-4.11), a direct relationship between the power coefficient and the thrust coefficient can be derived [Hansen, 2000, p.47].

$$C_P = \frac{1}{2}\left(1+\sqrt{1-C_T}\right)C_T \qquad \text{(III-4.12)}$$

This equation, plotted on Figure 21, is only valid for a C_T lower than *8/9*, as it corresponds to the "limit" of *a=1/3*, measured by Glauert. For higher values, the empirical correction of Glauert and Lockes

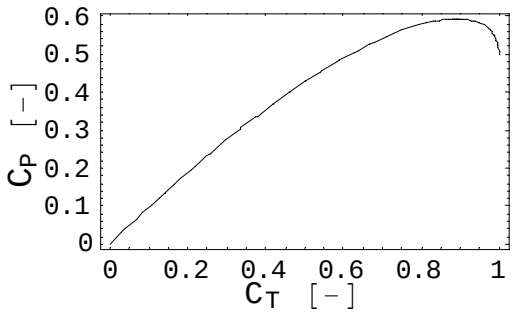

Figure 21: Relationship between C_P and C_T.

A4 Rotation of the wake

The horizontal axis wind turbines extract energy by the rotation of their rotor around an axis parallel to the incoming flow. A torque, associated to the thrust, is therefore applied on the rotor shaft, and used to collect the energy. Following the Newton rule of action/reaction, an equal opposite torque is therefore applied on the flow passing through the rotor disc, which creates a rotation of the wake.

The additional tangential velocity of the flow in the wake is drawn from a loss of pressure at the disc surface, which comes in addition to the one previously found. Similarly as for the axial velocity change, the change in tangential velocity can be represented by a tangential induced velocity factor *a'*. The tangential velocity is null at the entrance of the control volume, far upstream the turbine, and gradually increases until behind the surface of the disc where it is equal to $2\Omega r a'$, where r is the distance from the center of the disc. At the middle of the actuator disc thickness, the induced tangential velocity is $\Omega r a'$ [Burton et al., 2001; Sharpe, 2003].

Different interpretations of the origin of the wake rotation energy were proposed. Glauert, when he developed his theory about windmills and fans [Glauert, 1935], assumed that the energy is an additional loss that reduces the amount of energy that can be extracted from the flow, i.e. that the energy is drawn from the flow going through the actuator disc. This assumption is refuted by de Sharp [2003], who stated that this energy is drawn from a gradient of pressure in the wake that is independent from the energy extraction, as it is still present at the outflow surface of the control volume. This gradient of pressure will be recovered through the work of the shear forces of the undisturbed flow on the wake rotation after the expansion of the wake. So in other words, the energy would be drawn from the undisturbed flow. Nonetheless, the difference of maximum power that the turbine can extract, considering or not this rotation, is found to be very small for high tip speed ratio, like the one used on most of the industrial wind turbines.

In order to compute the relationship between *a* and *a'*, the angular momentum theory can be used. It states that the torque applied by the flow on the shaft must be equal to the rate of change of angular momentum. This angular momentum is dependant of the distance from the center of the shaft, so an integration has to be done to compute the total torque. The angular momentum can also be expressed on an annular ring centered around the shaft: the change of tangential velocity from before to after the shaft multiplied by the mass flow rate and by the radius (III-4.13), with Ω the rotation speed, and δA the .

$$\delta Q = 2\Omega a' r \cdot \rho U_\infty (1-a)\delta A \cdot r \qquad \text{(III-4.13)}$$

If the area of the annular ring is defined as (III-4.14).

$$\delta A = 2\pi r \delta r \qquad \text{(III-4.14)}$$

Equation (III-4.13) becomes

$$\delta Q = 4\pi \rho \Omega (1-a) a' U_\infty r^3 \delta r \qquad \text{(III-4.15)}$$

The corresponding increment of rotor shaft power output is related to the increment of torque and the rotation speed ($\delta P = \delta Q \cdot \Omega$), which leads to an expression of the increment of power

$$\delta P = 4\pi\rho\Omega^2\left(1-a\right)a'U_\infty r^3\,\delta r \tag{III-4.16}$$

The results found in the simple actuator disc model are still valid: the power derived through the conservation of kinetic energy of the axial velocity is the same as the one derived using the torque (III-4.17), which leads to a relation between the axial induction factor *a*, and the tangential induction factor *a'* (III-4.18).

$$4\pi\rho\Omega^2\left(1-a\right)a'U_\infty r^3\,\delta r = 4\pi\rho r\,a\left(1-a\right)^2 U_\infty^3\,\delta r \tag{III-4.17}$$

$$a' = a\left(1-a\right)\frac{U_\infty^2}{\Omega^2 r^2} \tag{III-4.18}$$

The wake rotation creates an additional loss of static pressure in the wake which is estimated as (III-4.19) [Burton, 2001, p.50].

$$\Delta p\left(r\right) = \frac{1}{2}\rho\left(2\Omega a' r\right)^2 \tag{III-4.19}$$

Or

$$\Delta p\left(r\right) = 2\rho a^2\left(1-a\right)^2\frac{U_\infty^4}{\Omega^2 r^2} \tag{III-4.20}$$

The additional thrust generated by this difference of pressure is then easily derived by multiplying by the annular area (III-4.14).

$$\boxed{\delta T_{add} = \Delta p\left(r\right)\delta A = 4\pi\rho a^2\left(1-a\right)^2\frac{U_\infty^4}{\Omega^2 r}\delta r} \tag{III-4.21}$$

This additional thrust does not extract power and should therefore be subtracted from the thrust coefficient used to express the power coefficient produced by the turbine. So from equation (III-4.12)

$$\boxed{C_P = \frac{1}{2}\left(1+\sqrt{1-\left(C_T - C_{T_{wake}}\right)}\right)\left(C_T - C_{T_{wake}}\right)} \tag{III-4.22}$$

The actuator disc theory paves the way to the Blade Element Method (BEM) designed by Glauert. Using further assumptions, the blade geometry and airfoil data, a converging iterative process, computes the induction factors distribution *a* and *a'* with respect to the inflow wind speed and the position on the blade. After this, the power output and the different loads applied on the turbine can be computed easily by integrating the previous equations.

Appendix B
Combined Uncertainty

The Guide to the expression of Uncertainty in Measurement (***GUM***) presented by the International Organization for Standardization (ISO) [ISO, 1993], is proposing a general method to quantify the combined uncertainty of values derived from measurements through predefined models. The GUM was widely used in the creation of standards for measurements in the wind industry, in particular concerning for the uncertainty estimation encompassed in power measurements.

B1 Type A and B

The GUM separates the uncertainty into two categories: type *A* and *B*. A type *A* uncertainty is an uncertainty that can be estimated from series of repeated observations (using a standard deviation for example), while a type B uncertainty is evaluated using the available knowledge from various sources. For example, the uncertainty of the hub height from the sea level cannot be evaluated through statistics as there are no information concerning the wave height, therefore the uncertainty is of type *B*, and should be evaluated from general knowledge about the tides in the area of the offshore wind farm. On the other hand, the power can be measured, and so the uncertainty of the power is of type *A,* and can be estimated with a standard deviation of the time series. While their origine are different, a type *A* and *B* uncertainty are used in the same way to compute the combined standard uncertainty of the measurement.

B2 Combined standard uncertainty of uncorrelated quantities

The combined standard uncertainty $u_c(y)$ is then defined as the positive square root of the combined variance $u_c^2(y)$ derived from equation (IV-1.1) for uncorrelated quantities, where *F* is the function which determines the measurand *Y* from *N* different quantities X_i: $Y = F(X_1, X_2, ..., X_N)$; and where $u(x_i)$ is the uncertainty of the quantity X_i, which can be of type *A* or type *B*.

$$u_c^2(y) = \sum_{i=1}^{N} \left(\left| \frac{\partial F}{\partial x_i} \right| \cdot u(x_i) \right)^2 \qquad \text{(IV-1.1)}$$

The term $\partial F / \partial x_i$ is called the sensitivity coefficient, and describes the importance of the quantity X_i in the final result of the measurand *Y*. It can be computed analytically from equation (IV-1.2), as the partial derivative of the function F with respect to the quantity X_i, using the estimates (mean values) of all the quantity as input.

$$\frac{\partial F}{\partial x_i} = \left.\frac{\partial F}{\partial X_i}\right|_{x_1, x_2, ..., x_N} \quad \text{(IV-1.2)}$$

The sensitivity coefficient can also be calculated numerically through the estimation of $\left|\partial F / \partial x_i\right| u(x_i)$ using equation (IV-1.3).

$$\left|\frac{\partial F}{\partial x_i}\right| u(x_i) = \frac{1}{2}\left|F(x_1, x_2, ..., x_i - u(x_i), ..., x_N) - F(x_1, x_2, ..., x_i + u(x_i), ..., x_N)\right| \quad \text{(IV-1.3)}$$

B3 Combined standard uncertainty of correlated quantities

If the quantities have a significant correlation, this should be taken into account in the derivation of the combined standard uncertainty. An extra term related to the correlation coefficient of the quantities should be added on top of equation (IV-1.1), where $r(x_i, x_j)$ is the correlation coefficient of the quantities X_i and X_j which can vary from -1 to 1 and is null for uncorrelated values.

$$u_c^2(y) = \sum_{i=1}^{N}\left(\left|\frac{\partial F}{\partial x_i}\right| \cdot u(x_i)\right)^2 + 2\sum_{i=1}^{N-1}\sum_{j=i+1}^{N}\frac{\partial F}{\partial x_i}\cdot\frac{\partial F}{\partial x_j}\cdot u(x_i)\cdot u(x_j)\cdot r(x_i, x_j) \quad \text{(IV-1.4)}$$

In practice, taking care of the correlation complexifies greatly the formulas, and is not always practical. The international standard IEC-61400-12, which deals with power measurement of wind turbines, proposes an interpretation of the GUM. In order to simplify the derivation of the combined uncertainty, the assumption is made that the components are whether fully correlated or fully uncorrelated. The standard goes even further by taking all the type A uncertainties as uncorrelated with one another, and with the type B uncertainties, while the type B uncertainties are taken as fully correlated across similar bins. The consequence for a power curve or a thrust curve is that, as the bins are not supposed to be similar (the wind speed is different for instance), there is no correlation to take into account.

B4 Estimation of type A uncertainties

Type A uncertainties are measured statistically from time series. In general, the data available are under the format of 10minute averaged time series, with optionally the corresponding standard deviation. According to the *Central Limit Theorem* [Wikipedia, Wolfram Research], the mean values of N independent time series of identical probability distribution are normally distributed whatever is the probability distribution of the time series. This amazing result also yields that the standard uncertainty of the mean of all the mean values considered is decreasing with the amount of data by a factor of $N^{-1/2}$. The standard uncertainty of the mean is equal to the standard deviation of the observations divided by the square root of the number of samples considered (IV-1.5).

$$u_A(\bar{X}) = \frac{std(X_i)}{\sqrt{N}} \quad \text{(IV-1.5)}$$

This result simplifies the uncertainty estimation of type A components: if the standard deviation of all the 10-minute average are assumed to be identical, the uncertainty of the mean of all the 10-minute is the standard deviation of the mean divided by the square root of the number of 10-minute average available. It is therefore not necessary to take into account the standard deviation of each 10-minute average. However, in order to be able to use this theorem, the standard deviation of each 10-minute considered should not be too different from the standard deviation of all the means. This is therefore used as a pre-process filter to keep only the data that are statistically similar.

This procedure can be justified as followed: if the standard deviation cannot be assumed identical, there is a parameter that plays a non-negligible influence on the results that is not taken into account in the analysis. Therefore making an average on this pool of data would not make sense statistically. If all the parameters are controlled, the remaining sources of deviation are whether biased errors, and taken into account within the type B uncertainties, whether random errors that should have an influence on the mean in relation with to the number of data available.

B5 Estimation of type B uncertainties

Type B uncertainties are estimated from general knowledge, or technical specification of the components. Their values can be fixed, or depend of other parameters. In general, in this report, the type of B uncertainties used are derived from boundaries encompassing the position of the mean. In that case, the associated standard uncertainty of the mean value is (IV-1.6), with a the radius of the boundary [ISO, 2003, p.13].

$$u(x_i) = \frac{a}{\sqrt{3}} \tag{IV-1.6}$$